Basanite–Phonolite Lineages of the Teide–Pico Viejo Volcanic Complex, Tenerife, Canary Islands

G. J. ABLAY[1,2]*, M. R. CARROLL[1], M. R. PALMER[1], J. MARTÍ[2], AND R. S. J. SPARKS[1]

[1]DEPARTMENT OF GEOLOGY, UNIVERSITY OF BRISTOL, WILLS MEMORIAL BUILDING, QUEEN'S ROAD, BRISTOL BS8 1RJ, UK

[2]CONSEJO DE INVESTIGACIONES CIENTIFICAS, INSTITUTE OF EARTH SCIENCES 'JAUME ALMERA' MARTI I FRANQUES S/N, 08028 BARCELONA, SPAIN

The petrology, geochemistry and petrogenesis of the active Teide–Pico Viejo volcanic complex provide information about the evolution and internal structure of the Tenerife central magma system during its most recent volcanic cycle. Two petrologically distinct basanite–phonolite lineages are identified, which correlate essentially with the products of the Pico Teide and Pico Viejo stratovolcanoes. Geochemical modelling supports the evolution of both series from a common evolved basanite parent, by crystal fractionation under different physico-chemical conditions. Pico Viejo series intermediate magmas fractionated mainly kaersutite and low-Or plagioclase at high P_{H_2O}, whereas Teide series examples fractionated mainly high-Or plagioclase and clinopyroxene at low P_{H_2O}, resulting in lower Ba, Sr, Eu/Eu* and MREE/HREE, and less peralkaline phonolitic residua. The Pico Viejo series shows smooth modal, mineralogical and whole-rock chemical variations, whereas the Teide series shows the additional effects of mineral accumulation, magma mixing, assimilation of hydrothermally altered crust and contamination by felsic magmas. Pyroxene barometry suggests that parental basanites and Pico Viejo series intermediate magmas evolved in the lower crust and uppermost mantle at 6–12 kbar P_{total}. Teide series intermediate magmas experienced polybaric fractionation, also differentiating extensively within a shallow chamber beneath Teide, where low P_{H_2O} conditions resulted from low P_{total} and, on the basis of F and Cl systematics, from open-system degassing. Hygrometry and melt-inclusion data from phonolites suggest a shallow Teide chamber at ~1·5 kbar P_{total}, whereas Pico Viejo series phonolites evolved in a separate shallow chamber at ~1 kbar P_{total}.

INTRODUCTION

Tenerife, the largest volcanic island of the Canary archipelago (Schmincke, 1982; Araña & Ortiz, 1991), provides an opportunity to study the effects of shallow-level processes on the evolution of phonolitic magmas in a long-lived, crustal magmatic system. Detailed geological and geophysical studies offer a robust framework within which to interpret the petrological evolution of the Tenerife system during its most recent cycle of activity. This activity has constructed two basanite–phonolite stratovolcanoes, Teide (3718 m) and Pico Viejo (3103 m), and numerous satellite vent systems collectively forming the Teide–Pico Viejo (T–PV) volcanic complex (Ridley, 1970; Araña *et al.*, 1989; Ablay, 1997). In this paper, we document the petrography, mineralogy and whole-rock chemistry of the T–PV volcanics, allowing the petrological evolution of the T–PV magma system to be assessed. Two distinct magmatic lineages are recognized; closely related in space and time and corresponding essentially to the products of Teide and Pico Viejo. The systematic differences between the lineages are interpreted to reflect their evolution from a common parental magma under contrasting physico-chemical conditions. In particular, water pressure (P_{H_2O}) is inferred

to have exerted a strong influence by controlling the relative stability of amphibole in the two series. This conclusion is supported by estimates of pre-eruptive conditions based on mineral–mineral and mineral–melt equilibria. The present study demonstrates the influence of shallow-level processes of fractionation, assimilation, magma mixing, contamination and degassing on the evolution of ocean island magmas, allows better evaluation of the deeper mantle signature, and places constraints on the internal structure and recent evolution of the Tenerife magmatic system.

Geological background

Tenerife consists of a central volcanic complex (Fig. 1) resting upon a composite mafic alkaline shield (Ancochea *et al.*, 1990; Martí *et al.*, 1994). The central complex consists largely of the Las Cañadas volcano, a composite stratovolcanic edifice consisting of a dominantly mafic to intermediate Lower Group (3·5–2·2 Ma), and an Upper Group comprising the products of three felsic volcanic cycles, the Ucanca (1·59–1·18 Ma), Guajara (0·85–0·65 Ma), and Diego Hernàndez (0·37–0·175 Ma) formations (Martí *et al.*, 1994). Each Upper Group cycle was terminated by a caldera collapse episode associated with felsic pyroclastic eruptions and followed by a migration in the focus of eruptive activity (Martí *et al.*, 1994, 1997). These destructive events formed the Las Cañadas caldera (Fig. 1), within which renewed activity since the most recent collapse at 175 ka (Mitjavila & Villa, 1993) has constructed Teide, Pico Viejo and numerous satellite vent systems. The most notable satellite system is Montaña Blanca, which produced a substantial subplinian phonolitic eruption at ~2 ka (Ablay *et al.*, 1995).

Teide–Pico Viejo complex

The lithostratigraphy of the T–PV complex is summarized in Table 1. It consists of a thick succession of mafic lavas, the Caldera Floor member (unit cf^1), overlain by intermediate to felsic lava sequences from Teide, Pico Viejo and Montaña Blanca (Fig. 1). The intermediate–felsic rocks will be shown to form two lineages which correlate with the products of (1) Teide and its satellite vents, and (2) Pico Viejo and its satellite vents. However, the oldest Pico Viejo lavas (units $pv^{2,3}$), resemble older Teide products more than younger products of Pico Viejo, suggesting that Pico Viejo developed initially as a satellite vent of the Teide sub-system. Products erupted from the two magmatic sub-systems are termed the Pico Teide series (PTS) and Pico Viejo series (PVS). The compositional ranges of T–PV rocks, classified using the total alkalis–silica scheme (Le Bas *et al.*, 1986), with nomenclature after Le Maitre (1989) are shown in Fig. 2.

The intermediate to felsic volcanics were erupted over four main episodes (Ablay, 1997), with activity alternating between Teide and Pico Viejo (Table 1). Each episode ended with phonolite eruptions and summit collapse at the active central vent. The first and most voluminous episode, PTS-1, saw the construction of Teide and the older part of Pico Viejo by intermediate lavas (units t^1, $pv^{2,3}$) and culminated with felsic eruptions from Teide flank vents (unit tf^1), including Montaña Blanca (unit ab^1). PTS-1 ended with hybrid lava flows from Teide (units $t^{1a,1b}$), and summit collapse. PVS-1 produced a succession of increasingly felsic lavas (units $pv^{4–7}$), and ended with the first summit caldera collapse of Pico Viejo, into which intermediate lavas were erupted (unit $pv^{8,9}$). PTS-2 involved central vent eruptions of hybrid lavas (unit t^2) and ended with another collapse of Teide. PVS-2 involved phonolite eruptions which occurred largely from Montaña Blanca (units $mb^{1–4}$). The Upper Montaña Blanca member (units $mb^{2–4}$) is the product of the ~2 ka eruption, which also occurred from Pico Viejo where a second caldera collapse occurred (Ablay *et al.*, 1995). Basanite eruptions have occurred outside the Las Cañadas caldera throughout the evolution of the T–PV complex, mainly in zones to the northwest and northeast. Historic eruptions of basanite occurred in 1430, 1704–1705, 1706 and 1909 (Fig. 1), and hybrid basanite–PVS phono-tephrite lava (unit pv^{12}) was erupted from Pico Viejo in 1798. Phonolite lava was erupted in historic times from Teide (unit t^3), probably in 1492 (Soler *et al.*, 1984).

PETROGRAPHY AND MINERALOGY

Representative samples of all major exposed units were examined, plus six samples collected from a hydrological gallery excavated into the lower part of the Pico Viejo edifice. Gabbro and syenite clasts from explosion deposits on Pico Viejo (units $pv^{10,13}$) were also investigated. Petrographic data for historic basanites have been given by Garcia-Moral (1989) and Cabrera (1981). Ten phenocryst phases were observed in the volcanic rocks: olivine (ol), clinopyroxene (cpx), plagioclase (plag), apatite (ap), kaersutite (kr), titano-magnetite (mt), ilmenite (ilm), alkali feldspar (afsp), biotite (bt) and titanite (titan). Nepheline, sodalite and secondary analcite occur in cogenetic syenites. Modal data on phenocryst contents and proportions for 57 samples have been reported by Ablay (1997). Phenocryst assemblages are summarized in Fig. 3.

Mafic rocks

Mafic rocks comprise magnesian (>7 wt % MgO) and evolved types (5–7 wt % MgO). T–PV mafic rocks (unit cf^1) are magnesian alkali basalts (2–7% normative ne) and
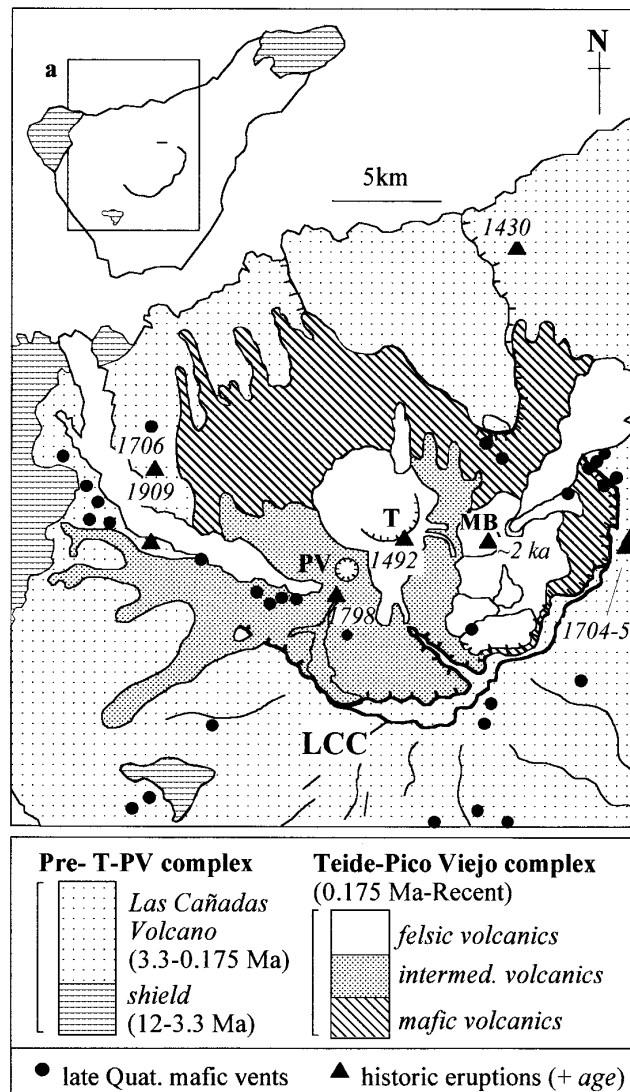
Fig. 1. Geology of central Tenerife showing the Teide–Pico Viejo complex, Las Cañadas Caldera (LCC) and Las Cañadas volcano. Inset (a) shows area of main map, caldera wall and locations of shield massifs (dark). Major T–PV vents, Teide (T), Pico Viejo (PV) and Montaña Blanca (MB) are labelled. Historic eruptions (with dates) are also shown.

basanites (10–16% ne), containing 9–16% phenocrysts of ol + cpx ± mt. Historic magnesian basanites (1430, 1704–1705 and 1706 eruptions) are petrographically similar to T–PV basanites, whereas historic evolved basanites (1430, 1706, 1798 and 1909) contain phenocrysts of ol + cpx + mt ± plag ± ap ± kr. More silica-rich basanites are termed plagioclase basanites.

Pico Viejo series

PVS lithologies are generally glassy with low crystal contents (0–14%), and phenocryst assemblages showing systematic variations in proportions and compositions. Plagioclase basanites (units pv[4,9]) contain phenocrysts of plag + ap + ilm, in addition to cpx + mt + rounded ol (Fig. 3a). Phono-tephrites (units pv[4,12]) contain kr in similar proportions to cpx and plag, with mt and rounded ol. Tephri-phonolites (units pv[5,6]) contain kr as the dominant mafic phase, with diopsidic cpx replaced by salite. Phonolites of units pv[7] and mb[1-4] are dominated by afsp, and also contain bt + mt + ilm + titan ± corroded kr. Phono-tephrites of unit pv[8] contain 55–63% crystals of plag + cpx + mt + ol + ap, in a well-crystallized groundmass of afsp + cpx + mt + ol.

Table 1: Litho-stratigraphy of the Teide-Pico Viejo complex [after Ablay (1997)]

Episode	Member	Unit	Lithology	Volume (km³)
historic	histor. basan. (1430, 1704–1705, 1706, 1909)*	—	basanite	~1
	PV (1798)*	pv^{12}	phonolitic tephrite, evolved basanite†	<0·01
	PT (1492)*	t^3	phonolite	~0·4
PVS 2	Upper MB	mb^{2-4}	phonolite	~0·12
	Lower MB	mb^1	phonolite	~0·22
PTS 2	PT Cone 2	mc^2	tephritic phonolite	~1·5
		t^2	phonolitic tephrite–phonolite†	
PVS 1	Pico Viejo caldera-fill	pv^9	plagioclase basanite	<0·01
		pv^8	phonolitic tephrite	~0·1
	PV upper cone	pv^7	phonolite	~0·32
		pv^6	teph. phonolite	~0·02
		pv^5	teph. phonolite	~0·4
		pv^4	plag. basanite, phonolitic tephrite	~1
PTS 1	PT cone 1	t^{1b}	phonolitic tephrite–phonolite†	<0·01
		t^{1a}	crystal-rich tephritic phonolite	<0·01
	PT flank vents	mc^1	crystal-rich tephritic phonolite	~1·7
		ab^1	phonolite	
		tf^{1a}	phonolite pumice	
		tf^1	trachy-phonolite, phonolite	
	PV lower cone	pv^3	phonolitic tephrite, tephritic phonolite	~3
		pv^2	plagioclase basanite	
	PT cone 1	t^1	phonolitic tephrite, tephritic phonolite	~10
Early	Caldera floor	cf^1	primitive basanite, alkali basalt	~30

*Historic flows (not members).
†Mingled lithologies.
PT, Pico Teide; PTS, Pico Teide series; PV, Pico Viejo; PVS, Pico Viejo series; MB, Montaña Blanca.

Pico Teide series

Olivine is more persistent in PTS intermediate rocks whereas kr is absent or rare, and titanite is absent from PTS phonolites (Fig. 3b). Older intermediate rocks (units $pv^{2,3}$, t^1) are crystal-rich (13–40 vol. %) glassy lavas ranging in composition from plagioclase basanite to tephri-phonolite. All are coarsely porphyritic (2–15 mm) and contain the phenocryst assemblage plag (6–35 vol. %) + cpx (1–19 vol. %) + mt + ol + ap ± ilm. Inter-mediate lavas collected from the hydrological tunnel are hydrothermally altered, with zeolite minerals in micro-fractures.

Younger intermediate rocks (units $t^{1b,2}$) include glassy phono-tephrites and tephri-phonolites, less crystal rich (8–12%) and finer grained (1–5 mm) than older products. Mineral assemblages comprise coexisting populations of skeletal Ca-plag and resorbed Na-plag (see Kawamoto, 1992), titanian diopside and diopsidic salite, and high-Mg and low-Mg titano-magnetite, with ap, anhedral ol and minor kr. Streaky groundmasses contain crystals of plag + cpx + mt + ol, and 2–5% of dark, non-vesicular, glassy mafic inclusions (<5 mm) containing 20–40% crystals of ol + cpx + plag + mt + ap ± kr.

Crystal-rich tephri-phonolites of unit tf^{1a} contain 35–65% phenocrysts (<5 mm) including coexisting skeletal plag and resorbed afsp, diopsidic salite and salite, and high-Mg and low-Mg titano-magnetite, with ap, anhedral ol and rare resorbed kr. They also contain 1–5% of glassy, vesicular mafic inclusions (<10 mm) with 40–70% crystals of ol + cpx + plag + ap + ilm. Rare holo-crystalline inclusions (<5 mm) of syeno-gabbro (plag + cpx + ol + mt + ap) and syenite (afsp + mt + ap ± ol) also occur.

PTS phonolites (units tf^1, ab^1, t^{1b}, t^2) are glassy to pilotaxitic rocks containing phenocrysts of afs + cpx + mt + bt + ap ± ilm ± kr. Afsp forms 80–90% of the phenocrysts. Trachy-phonolites of units tf^1 and t^2 contain only rounded crystals of afsp ± mt. Unit t^3 phonolites are glassy, porphyritic rocks (17–38% crystals) containing afsp + cpx + mt + ap.
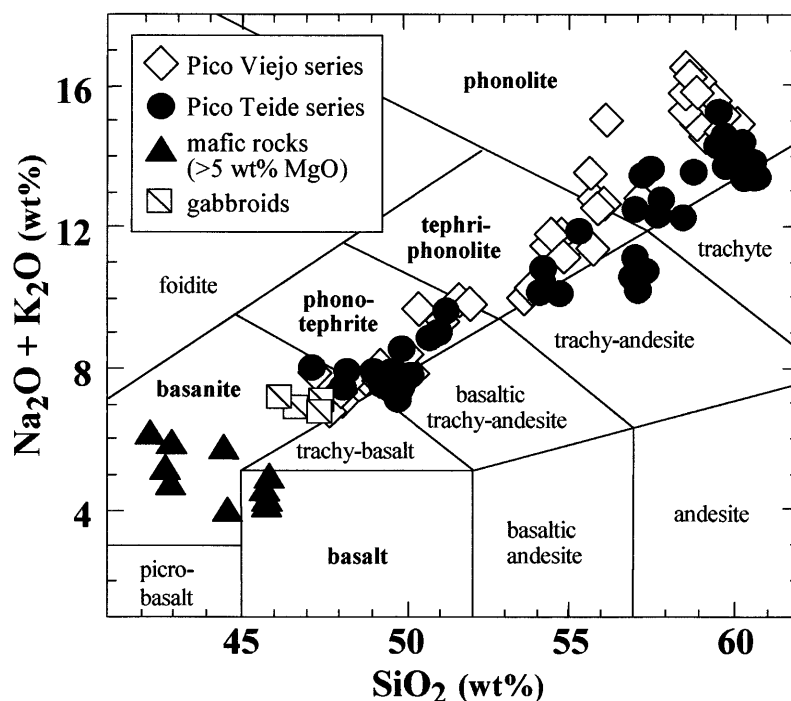
Fig. 2. Total alkalis–silica classification diagram (Le Bas *et al.*, 1986), nomenclature after Le Maitre (1989). T–PV 'mafic' products (>5 wt % MgO) include basanites (10–16% ne) and alkali basalts (2–7% ne), all of which lack plagioclase phenocrysts. More silica-rich plagioclase-phyric basanites of the PTS and PVS are termed plagioclase basanites. Plagioclase basanite to tephri-phonolite compositions are termed 'intermediate'. Rocks falling in the basaltic trachy-andesite and trachy-andesite fields are called phono-tephrite or tephri-phonolite. 'Felsic' rocks are mostly mildly peralkaline phonolites. Those falling within the trachyte field are termed trachy-phonolites.

Mineralogy

Electron microprobe analyses were performed using a JEOL JXA-8600*a* Superprobe with Link Analytical AN10/85s analyser and LEMAS automation at Bristol University. Analysis was by wavelength dispersive methods at an accelerating voltage of 15 kV, beam current 15 nA, and beam diameter 2–20 μm. Full microprobe analyses may be freely accessed from an electronic data repository at www1.gly.bris.ac.uk/cetsei/resources.html.

Olivine

Analysed olivines range from Fo_{79-86} in T–PV mafic lavas to Fo_{83-64} and Fo_{73-59} in PVS and PTS lavas, respectively. Fe-rich olivine (Fo_{60-52}; <2·8 wt % MnO) occurs in unit pv^8, unit t^{1a} syeno-gabbros and unit mb^3 banded pumices.

Clinopyroxene

T–PV clinopyroxenes are highly calcic and show modest variations in Wo–En–Fs but large variations in non-quadrilateral components. Those from basanite to tephri-phonolite rocks vary from violet–brown, aluminous titanian diopside ($Wo_{41-44}En_{46-52}Fs_{8-11}$), to beige diopsidic salite ($Wo_{45-49}En_{45-42}Fs_{9-14}$), with decreasing Al^{IV}, Al^{VI}, Ti, Cr, Fe^{3+} and Ni, increasing Mg, Fe^{2+}, Mn and Si, and

minor Mg–(Fe^{2+}, Mn) substitution. PTS diopsides have systematically higher Sr and Ba than PVS examples. Felsic rocks contain green salite ($Wo_{45-47}En_{37-41}Fs_{11-18}$), which in PVS examples is separated from diopsidic salite by a compositional gap. Salites exhibit low Al, Ti, Cr and Ni, extensive [Fe^{2+}, Mn, Fe^{3+}]–Mg substitution, and ~1 wt % Na_2O. Cogenetic syenites host sodic ferro-salites with <12 wt % Na_2O.

Amphibole

Kaersutite is common in the PVS, but rare or absent in the PTS. T–PV kaersutites are rich in Mg, Ti, Ti^{IV}, Fe^{3+}, Ca, Na and Al, and poor in Si and K compared with those from other alkaline series (e.g. Kyle *et al.*, 1992), and show a slight decrease in Mg, Ba and Sr, and increases in Fe^{2+} and Ca as host rocks become more felsic. F contents (~0·4 atoms p.f.u.) are highest in unit pv^5 (0·94 p.f.u.). Cl contents are negligible. Breakdown rims on kr crystals from some samples comprise mt + ilm + cpx ± bt ± sulphides.
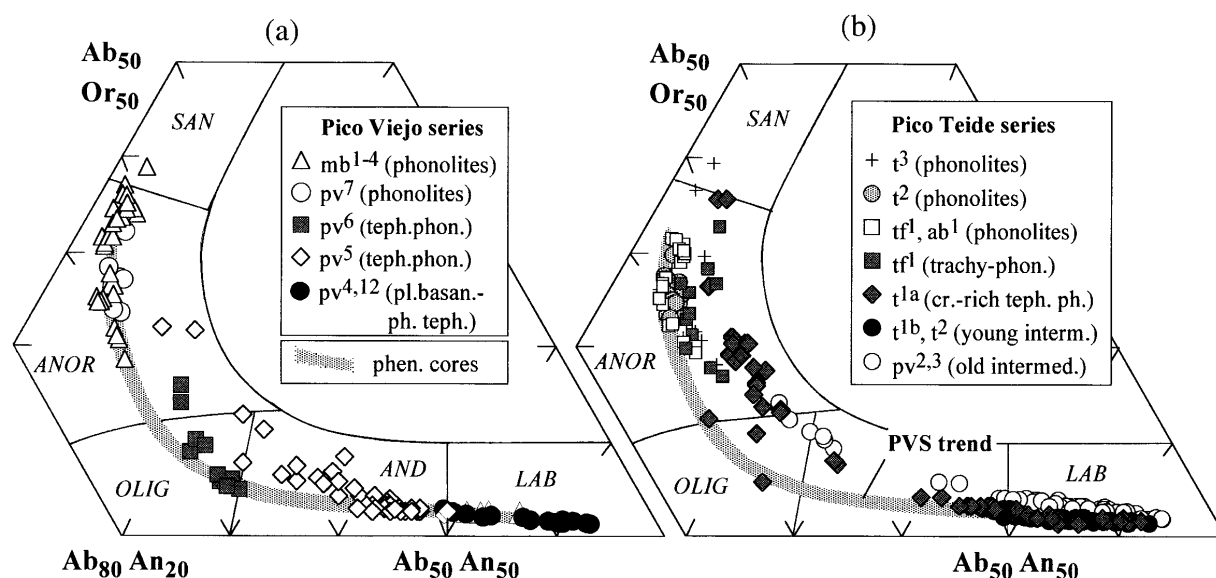
Feldspar

Non-hybrid T–PV rocks contain feldspars which vary continuously from plagioclase to alkali feldspar. PTS
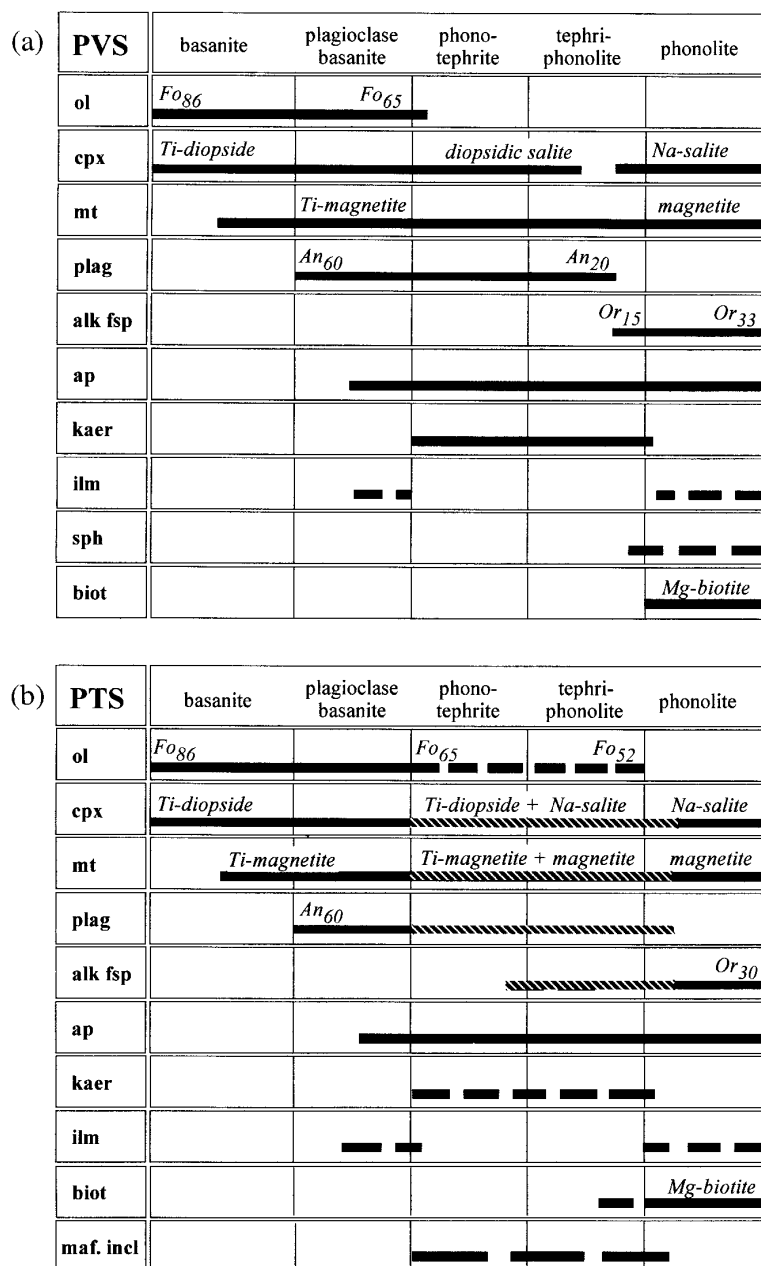
Fig. 3. Generalized variations in phenocryst assemblage with composition for (a) Pico Viejo series and (b) Pico Teide series. Thick continuous lines indicate that a particular phase is present. Broken lines indicate that a phase may be absent, or is present in trace amounts. Diagonal hatched lines indicate multiple populations of a phase with contrasting compositions. The presence of mafic inclusions in PTS lithologies is also indicated.

feldspars have higher minor element (Sr, Ba, Fe^{3+}) contents than PVS feldspars of similar An content. Figure 4a shows that feldspar core compositions from PVS rocks vary systematically as the host becomes more evolved. Rim and groundmass compositions have higher [Or + Ab]/An. Feldspar cores from PTS intermediate rocks show contrasting high-Or and low-Or trends which correspond to the older and younger groups (Fig. 4b). Older PTS intermediate rocks contain coarse, high-Or plagioclase. Labradorites from unit pv^2 plagioclase basanites show a calcium spike, being normal zoned from An_{52} cores to skeletal rims reverse zoned from An_{62} to An_{53}. Younger phono-tephrites contain three feldspar types: (1) skeletal, normal-zoned plagioclase (An_{53-}

Fig. 4. Feldspar compositions in the albite-rich part of the feldspar ternary. LAB, labradorite; AND, andesine; OLIG, oligoclase; ANOR, anorthoclase; SAN, sanidine. (a) Pico Viejo series; shaded field shows the compositions of phenocryst cores. (b) Pico Teide series; high-Or and low-Or trends should be noted. Shaded field shows the compositions of PVS phenocryst cores for comparison.

$_{60}Or_2Ab_{45-38}$); (2) resorbed sodic plagioclase ($An_{30-48}Or_{9-3}Ab_{61-49}$); (3) euhedral plagioclase ($An_{52-54}Or_2Ab_{46-44}$), which rims other types. Mafic inclusions contain skeletal labradorite ($An_{60}Or_2Ab_{38}$). Crystal-rich tephri-phonolites (unit t^{1a}) contain diverse high-Or feldspar (Fig. 4b) showing complex zoning, mantling and resorption textures, whereas their mafic inclusions contain skeletal low-Or plagioclase. PTS phonolites (units tf^1, ab^1, t^2) contain weakly normal-zoned anorthoclase (Fig. 4b), whereas the trachy-phonolites contain more ternary alkali feldspar.

Iron–titanium oxides

Titano-magnetite compositions range from Usp_{75} to Usp_{28} as host rocks become more felsic. As Usp content decreases, Al, Mg and Cr fall, whereas MnO increases from 0·5–1·0 to 2–3 wt %. Ilmenite (Ilm_{90-97}) occurs only in some plagioclase basanites and phonolites, where it forms 0·1–10% of the total Fe–Ti oxides.

Biotite

Biotite phenocrysts occur in all phonolites except unit t^3, but are absent from trachy-phonolites. T–PV biotites are Mg and Ti rich with high Na, Ba and Sr, and low Si, Al and *y*-site occupancy. The compositional range is $An_{33-42}Ph_{58-74}$. Occupancy of OH sites by F is 3–18%. PTS biotites (units tf^1, ab^1, t^2) are richer in Mg, Ti, F and S than PVS biotites (units mb^{1-4}).

Apatite

Apatite forms small phenocrysts but occurs mainly as inclusions in clinopyroxene and/or amphibole. Most are hydroxy-fluorapatites with 1·1–2·8 wt % F, substantial Cl and some S. There is limited substitution of Mg, Fe^{2+}, Mn and Sr (2000–6000 ppm) for Ca. PTS apatites contain higher F, Cl, S, Sr and Ba than PVS apatites, which are OH rich.

Intensive parameters

Geothermometry

Olivine–liquid Ca–Mg exchange thermometry (Jurewicz & Watson, 1988) was applied to mafic rocks with equilibrium olivine–melt pairs (Roedder & Emslie, 1970). Results were compared with the clinopyroxene–liquid thermometer (T1) of Putirka *et al.* (1996). For more evolved, glassy rocks, temperature (T) and oxygen fugacity (f_{O_2}) were estimated from ilmenite–magnetite pairs (Sack & Ghiorso, 1991), which were checked for Mg–Mn equilibrium (Bacon & Hirschmann, 1988). Olivine thermometry yields 1230°C and 1210°C for two alkali basalts and 1180°C for an evolved basanite (all ±40°C). Clinopyroxene–liquid estimates are 1224°C, 1211°C and 1197°C, respectively, for the same rocks (all ±27°C). The T–PV rocks are reduced and define a T–f_{O_2} array oblique to natural buffers, becoming more reduced with differentiation (Fig. 5). The results suggest that the most An-rich PVS or PTS feldspars (An_{62}) from plagioclase
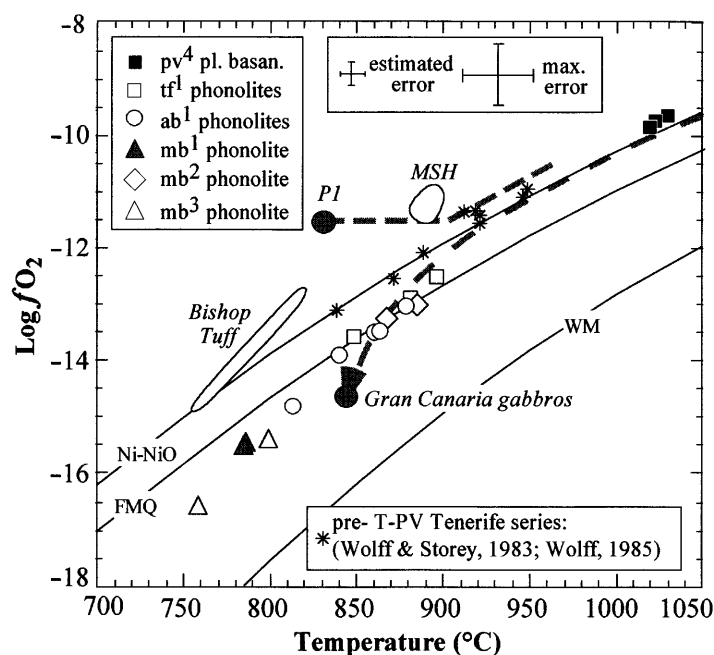
Fig. 5. Temperature–oxygen fugacity (f_{O_2}) relationships for Tenerife volcanic rocks from Fe–Ti oxides. Other rocks: Gran Canaria (Miocene series)—P1-ignimbrite (trachyandesite–trachyte), gabbros (Freundt & Schmincke, 1995), calc-alkaline felsic rocks; MSH—Mount St Helens dacites (Rutherford et al., 1985); Bishop Tuff rhyolites (Hildreth, 1979). Max. error—maximum microprobe errors propagated through calculation scheme (Sack & Ghiorso, 1991); estimated error—maximum discrepancy between four equilibrium oxide pairs from a single sample (T1-22-6) selected using Mg–Mn partitioning (Bacon & Metz, 1984; Bacon & Hirschmann, 1988). Oxygen buffers: Mn–MnO, Ni–NiO (NNO), W–M (wüstite–magnetite) (Eugster & Wones, 1962; Huebner & Sato, 1970), FMQ (fayalite–magnetite–quartz) (O'Neill, 1987).

basanites crystallized just above 1030°C. Bytownites ($An_{88–66}$) from historic basanites formed either above 1180°C or at high water activities (Brown, 1993). Alkali feldspar saturation is found to occur at ~890–900°C. Kaersutite crystallizes between 900 and 1020°C, whereas biotite is found to be stable between 760 and 900°C.

Geobarometry

The geobarometer of Grove et al. (1989) and P1 of Putirka et al. (1996), which is appropriate only for mafic compositions, were applied to analyses of euhedral pyroxene cores. The Grove et al. (1989) barometer was calibrated for plagioclase-saturated mid-ocean ridge basalt (MORB) and high-alumina basalt (HAB), not for silica-undersaturated or felsic compositions, and is suggested to yield only very approximate pressure estimates. Mafic T–PV rocks yield pressures of 7·5–9·1 ($\pm$ 1) kbar using Grove et al. (1989) and 9·7–11·6 ($\pm$ 1·4) kbar using Putirka et al. (1996). Intermediate PVS rocks from units pv[4,5,12] yield pressure estimates of 6·2–7·1 kbar using Grove et al. (1989), whereas felsic tephri-phonolite of unit pv[6] yields 4·5 kbar. Low-Al[VI] salites from PVS phonolites yield 2·5–2·9 kbar, qualitatively suggesting a low-pressure origin. PTS intermediate rocks yield estimates of 5·3–10·0

kbar. Pyroxene compositions from units t[2] (1·2–3·1 kbar) and t[3] (2·1–5·5 kbar) suggest low pressures.

Pre-eruptive f_{H_2O}

Compositions of coexisting sanidine, magnetite and biotite were used to estimate the water fugacity (f_{H_2O}) for several T–PV phonolite units (Wones & Eugster, 1965; Wones, 1972; Czamanske & Wones, 1973). From the discriminant plots of Righter & Carmichael (1996), site vacancies ([ ]) in T–PV biotites enter by coupled substitution of Ti + [ ] for 2[Mg,Fe], and Fe^{3+} was estimated assuming that it balances excess Al[IV] and alkalis (see Papike et al., 1974). Low estimated Fe^{3+} contents are consistent with low f_{O_2} (Hewitt & Wones, 1984). The small effect of Na on biotite stability (Rutherford, 1969) was ignored. OH⁻ was assumed to occupy all hydroxyl sites not filled by F. The activity of Or in sanidine was estimated graphically from Waldbaum & Thompson's (1969) alkali feldspar data (Carmichael et al., 1974), with An substitution ($\leqslant$4 mol%) ignored (see Parsons, 1981). The PTS Montaña Majua lava (unit tf[1]) yields f_{H_2O} = 950–1040 bars, whereas the associated pumice (unit tf[1a]) gives 1430–1570 bars. A PVS phonolite from unit mb[1] yields 920–1140 bars, similar to 950–1080 bars for unit mb[2]. Unit mb[3] pumice yields 690–700 bars.

Table 2: Volatile contents of selected melt inclusions from the Montaña Majua pumice (unit tf^1)

	1	2	3	4	5	6	7	8
H$_2$O (wt %)	1·15	0·76	2·18	2·49	0·95	0·29	0·77	0·14
F (ppm)	2430	3030	5480	2370	3380	1180	704	630
Zr (ppm)	818	940	643	948	288	436	3840	942

Key to analyses: 1–6, unleaked inclusions from salite grains; 7, inclusions with elevated Zr interpreted as a result of post-entrapment crystallization and rupture; 8, matrix glass. Analyst: Dr J. Barclay.

Pre-eruptive volatile contents

Salite phenocrysts from pumice contain glass inclusions (40–150 μm), which allow the pre-eruptive volatile content of the host magma to be assessed (see Anderson, 1974; Webster *et al.*, 1993). Glass inclusions from units tf^{1a} and mb^3 were analysed by ion microprobe for H, F and Zr. Details of sample preparation and analysis have been given elsewhere (Ablay *et al.*, 1995; Barclay *et al.*, 1996). Inclusion data indicate that unit mb^3 pumice-forming magma contained 3·0–4·5 wt % H$_2$O and ~3000 ppm F (Ablay *et al.*, 1995). For the Montaña Majua pumice (unit tf^1), inclusions have less H$_2$O (0·75–2·5 wt %) and greater F (2400–5500 ppm) than inclusions from unit mb^3 (Table 2). Inclusions with high Zr relative to the host glass, and low H$_2$O and F, are interpreted to have been affected by post-entrapment crystallization and leaked volatiles (Johnson *et al.*, 1994).

Estimates of P$_{H_2O}$ and P$_{total}$

For phonolitic pumice of units tf^1 and mb^3, the minimum total pressure (P_{total}) at which these magmas equilibrated may be estimated using f_{H_2O} data, fugacity coefficients (Holloway, 1987), melt inclusion H$_2$O contents, and the pressure dependence of H$_2$O solubility in Montaña Blanca phonolite (Carroll & Blank, 1997). For unit mb^3, an f_{H_2O} of 700 bars corresponds to a minimum P_{total} of 830 bars for H$_2$O saturation at 760°C. Assuming a pure H$_2$O fluid, the maximum H$_2$O solubility at P_{total} = 830 bars is 4·6 wt %. This is very close to the upper limit of melt-inclusion data, suggesting that unit mb^3 magma was near saturation with a water-dominated fluid at just over 830 bars total pressure. For the Montaña Majua pumice (unit tf^{1a}), an f_{H_2O} of 1500 bars corresponds to a P_{total} of 1765 bars for water saturation at 860°C. Melt inclusion H$_2$O contents of ~2·5 wt % would achieve saturation at ~370 bars, suggesting that either (1) the inclusions do not sample the most water-rich magma or have leaked, or (2) the f_{H_2O} estimate is too high.

WHOLE-ROCK GEOCHEMISTRY

One hundred and forty T–PV rocks were analysed for major and trace elements by X-ray fluorescence (XRF). A subset of 30 samples were analysed for rare earth elements (REE) by inductively coupled plasma mass spectrometry (ICP-MS). Representative analyses are given in Table 3. Further data for MB phonolites (units mb$^{1–4}$) and PTS phonolites have been reported by Ablay *et al.* (1995). Full whole-rock chemical analyses may be freely accessed from an electronic data repository at www1.gly.bris.ac.uk/cetsei/resources. Analyses of glassy and massive lava facies revealed no post-eruptive alkali loss (e.g. Noble, 1965). Three samples of older PTS intermediate lavas collected from a water tunnel (prefixed TPVG) are zeolitized and show evidence of chemical alteration; all other samples are fresh and unaltered.

Whole-rock chemical variations

As a group, the T–PV volcanics show the typical geochemical features of fractionation, with oxides compatible into the major ferro-magnesian phases (MgO, Fe$_2$O$_3$*, CaO) decreasing with increasing SiO$_2$ (Fig. 6). Compatible trace elements (Ni, Cr, Sc, Co) likewise decrease with MgO because of fractionation of ol and cpx. The onset of Fe–Ti oxide fractionation is marked by a decrease in TiO$_2$ (and V) at <8 wt % MgO (Fig. 7a). A strong decrease in P$_2$O$_5$ at <6 wt % MgO (Fig. 7b) reflects ap saturation. The entrance of plag causes subtle inflections in the trends of Al$_2$O$_3$ and Na$_2$O at ~48 wt % SiO$_2$ (<6 wt % MgO), and produces a maximum in Sr vs Ba (Figs 6 and 8). Na$_2$O, K$_2$O and Al$_2$O$_3$ increase with SiO$_2$ until the phonolites (58–61 wt % SiO$_2$), where SiO$_2$ and Al$_2$O$_3$ decrease and Na$_2$O/K$_2$O increases. These features are attributed to separation of afsp, which also produces a maximum in Ba (Fig. 8). Incompatible trace element contents (Zr, Nb, Rb, Cs, Th, Ta, Y) are high, as for other basanite–phonolite series (Le Roex *et al.*, 1990; Kyle *et al.*, 1992; Wilson *et al.*, 1995). Zr, Nb and Rb are enriched continuously from mafic to felsic rocks, whereas

Table 3: Selected whole-rock analyses

| Sample: | T4-21-7 | T-1909 | T2-31-1 | T2-28-1 | T5-4 | T1-17-4a | TPVG-1 | T1-18-10b | T3-17-2 | T1-18-9 | T2-27-10 |
Unit:	cf[1]	hist.	cf[1]	pv[2]	t[1]	pv[3]	t[1]	t[1b]	t[2]	t[1]	pv[9]
SiO_2	43·11	44·89	46·21	48·61	47·61	50·34	55·47	49·60	51·08	57·82	48·31
Al_2O_3	12·48	15·72	12·73	17·07	16·19	17·46	18·95	17·11	17·67	18·90	16·95
TiO_2	4·00	3·73	2·94	2·95	3·49	2·61	1·59	2·73	2·47	1·22	3·15
Fe_2O_3*	14·00	12·72	12·65	10·18	11·53	9·86	5·82	9·64	8·78	4·45	10·30
MgO	9·87	5·39	9·81	3·85	3·76	2·81	1·80	3·51	3·25	1·13	4·06
CaO	10·41	10·76	9·84	8·01	7·56	7·04	3·47	7·73	6·38	2·56	8·54
Na_2O	3·58	4·02	3·44	5·30	4·14	5·57	7·22	5·49	5·76	7·88	4·93
K_2O	1·58	1·66	1·41	2·46	2·62	2·84	4·62	2·37	3·08	4·87	2·19
MnO	0·18	0·19	0·17	0·18	0·23	0·18	0·15	0·22	0·20	0·16	0·17
P_2O_5	0·77	0·92	0·71	1·10	1·38	1·07	0·38	1·13	0·97	0·26	1·16
LOI	−0·40	−0·48	−0·48	−0·13	1·31	−0·28	0·25	−0·08	−0·08	0·38	−0·20
Total	99·58	99·52	99·43	99·58	99·82	99·50	99·72	99·45	99·56	99·63	99·56
Ba	428	465	507	836	997	881	815	720	866	955	663
Cl	262	215	244	230	0	207	908	340	718	1007	536
Co	—	43	54	25	—	25	—	23	—	10	28
Cr	311	33	333	12	11	6	11	21	18	0	9
F	1750	1326	635	948	3089	1095	1033	1776	1321	607	994
Nb	80	85	73	115	130	122	172	118	132	178	106
Ni	210	14	207	9	4	3	9	2	4	6	10
Pb	2	7	12	6	12	7	10	11	7	18	10
Rb	34	34	33	55	62	62	134	55	79	148	48
S	220	363	282	313	1889	570	186	177	231	464	286
Sr	935	1130	780	1144	1081	975	470	1259	1017	400	1183
Th	7	10	3	8	15	8	25	10	18	23	7
U	0	1	0	2	0	2	6	1	3	3	0
V	327	293	255	196	174	133	96	164	148	55	215
Y	27	35	28	38	48	46	28	43	39	31	38
Zr	266	292	251	371	434	427	696	406	481	751	351
La	—	48·80	40·70	67·82	—	—	—	—	—	83·10	—
Ce	—	104·12	84·8	136·07	—	—	—	—	—	146·08	—
Pr	—	12·14	9·70	14·91	—	—	—	—	—	13·96	—
Nd	—	45·17	34·19	52·62	—	—	—	—	—	42·10	—
Sm	—	8·36	6·81	9·61	—	—	—	—	—	6·86	—
Eu	—	3·00	2·47	3·29	—	—	—	—	—	2·21	—
Gd	—	7·64	6·43	8·46	—	—	—	—	—	5·65	—
Tb	—	0·95	0·77	1·11	—	—	—	—	—	0·77	—
Dy	—	5·37	4·38	5·99	—	—	—	—	—	4·55	—
Ho	—	0·91	0·71	0·95	—	—	—	—	—	0·81	—
Er	—	2·10	1·74	2·73	—	—	—	—	—	2·48	—
Tm	—	0·27	0·25	0·35	—	—	—	—	—	0·35	—
Yb	—	1·64	1·36	2·06	—	—	—	—	—	2·35	—
Lu	—	0·25	0·20	0·29	—	—	—	—	—	0·37	—

Table 3: continued

Sample:	T1-20-24	T1-23-7	T1-17-12	T5-16-7	T4-LLP	T1-27-4	T1-27-2	T1-17-2	T1-29-6	T1-21-0	T2-27-3
Unit:	pv[13]	pv[4]	pv[5]	pv[6]	pv[8]	tf[1]	tf[1]	t[2]	t[2]	t[3]	pv[6]
SiO_2	49·53	48·99	54·95	57·20	52·38	60·42	59·51	58·97	60·46	59·76	59·38
Al_2O_3	17·26	16·74	18·83	19·62	18·28	19·01	18·98	18·82	19·14	18·60	18·89
TiO_2	2·80	2·97	1·70	1·12	2·13	0·75	0·77	0·68	0·77	0·75	0·66
Fe_2O_3*	9·47	9·91	6·05	4·92	7·95	3·40	3·68	3·78	3·50	3·82	3·84
MgO	3·51	3·80	1·71	0·96	2·52	0·53	0·56	0·40	0·51	0·55	0·41
CaO	7·78	8·15	3·93	2·06	5·57	1·28	1·10	0·84	1·02	1·22	0·88
Na_2O	5·66	5·45	7·61	7·96	6·37	8·31	8·60	9·80	8·09	9·04	9·90
K_2O	2·41	2·22	3·80	4·80	3·42	5·19	5·34	5·43	5·36	5·16	5·48
MnO	0·20	0·19	0·21	0·18	0·18	0·15	0·19	0·20	0·17	0·17	0·19
P_2O_5	1·07	1·17	0·47	0·22	0·83	0·11	0·11	0·10	0·13	0·14	0·07
LOI	−0·18	−0·13	0·05	0·76	0·03	0·38	0·58	0·38	0·75	0·23	0·35
Total	99·51	99·46	99·31	99·80	99·66	99·53	99·42	99·40	99·90	99·44	100·05
Ba	648	640	1100	1349	998	1070	421	54	1047	711	31
Cl	562	1000	1960	1841	2237	1373	2649	3121	1466	2123	3326
Co	27	28	10	—	—	13	10	11	—	10	14
Cr	19	24	3	0	10	9	7	7	15	8	0
F	1217	1247	1107	796	1076	475	779	931	210	809	911
Nb	112	108	174	215	156	184	224	254	186	199	269
Ni	2	2	2	7	8	2	3	5	6	2	7
Pb	10	10	12	17	14	16	19	20	16	21	21
Rb	54	53	96	132	99	152	171	179	153	143	185
S	174	120	432	150	85	91	115	163	102	221	161
Sr	1128	1177	892	430	1119	123	34	4	70	134	6
Th	9	8	17	27	22	28	29	30	25	26	29
U	3	1	2	7	4	6	5	6	7	4	8
V	177	190	73	35	111	27	29	24	31	25	18
Y	40	41	40	39	38	31	42	46	28	37	44
Zr	396	380	587	770	578	816	941	1084	832	798	1114
La	71·86	72·64	88·65	—	—	126·41	48·18	98·65	—	82·21	—
Ce	146·21	146·64	164·95	—	—	117·21	105·25	176·72	—	147·94	—
Pr	16·46	16·41	16·75	—	—	10·81	9·79	16·7	—	13·85	—
Nd	57·62	57·61	53·17	—	—	31·62	29·18	50·4	—	40·43	—
Sm	10·54	10·04	8·63	—	—	4·94	4·79	8·08	—	6·23	—
Eu	3·40	3·361	3·16	—	—	1·58	1·25	1·59	—	1·78	—
Gd	9·14	9·88	7·62	—	—	4·28	4·53	6·89	—	5·92	—
Tb	1·19	1·14	1·00	—	—	0·64	0·61	0·99	—	0·81	—
Dy	6·45	6·33	5·78	—	—	3·43	3·77	5·92	—	4·54	—
Ho	1·04	1·11	0·98	—	—	0·66	0·67	1·15	—	0·88	—
Er	2·89	2·97	2·79	—	—	1·87	2·16	3·31	—	2·64	—
Tm	0·35	0·39	0·38	—	—	0·32	0·30	0·52	—	0·35	—
Yb	2·07	2·28	2·41	—	—	2·10	2·30	3·26	—	2·39	—
Lu	0·31	0·31	0·38	—	—	0·35	0·40	0·58	—	0·40	—

Major elements in wt %, trace elements in ppm (all raw data); major and trace elements by XRF; rare earth elements by ICP-MS. Fe_2O_3*, all Fe as Fe^{3+}; LOI, loss on ignition.
Sample descriptions: T4-21-7, magnesian basanite; T-1909, evolved basanite; T2-31-1, magnesian alkali basalt; T2-28-1, PTS plagioclase basanite; T5-4, PTS gabbro; T1-17-4a, PTS phono-tephrite; TPVG-1, PTS tephri-phonolite; T1-18-10b, PTS phono-tephrite; T3-17-2, PTS tephri-phonolite; T1-18-9, PTS crystal-rich tephri-phonolite; T2-27-10, PVS plagioclase basanite; T1-20-24, PVS phono-tephrite; T1-23-7, PVS plagioclase basanite; T1-17-12, PVS mafic tephri-phonolite; T5-16-7, PVS felsic tephri-phonolite; T4-LLP, PVS phono-tephrite; T1-27-4, PTS high-Ba trachy-phonolite; T1-27-2, PTS phonolite; T1-17-2, PTS evolved phonolite; T1-29-6, PTS high-Ba trachy-phonolite; T1-21-0, PTS phonolite; T1-27-3, PVS phonolite.

Y shows inflections caused by ap and afsp saturation (Fig. 9a–c).

Pico Teide series and Pico Viejo series

PTS and PVS intermediate rocks show similar major element variations (Fig. 6). Greater scatter among the PTS can be attributed to accumulation of phenocrysts. PTS phonolites and trachy-phonolites are generally poorer in Na_2O and richer in SiO_2, K_2O and Al_2O_3 than phonolites of the PVS (Fig. 6). Certain trace elements (Ba, Sr, Rb, Zr, Nb, Y) also show significant contrasts. The PTS shows less enrichment in Ba and greater depletion in Sr than the PVS (Fig. 8). The PTS deviates more from constant incompatible element ratios such as Zr/Nb = 3·43 and Nb/Rb = 1·95, and PTS rocks have generally lower Y contents than PVS examples (Fig. 9a–c). The two series also exhibit contrasting halogen variations (Fig. 10). Both series are poor in F, except for P_2O_5- and Y-rich PTS plagioclase basanites (unit pv[2]), which are interpreted to have accumulated fluorapatite. F contents from pristine melt inclusions in phonolites of both series are also comparable (Fig. 10a). However, PVS intermediate products have systematically higher Cl contents than PTS examples (Fig. 10b).

Rare earth elements

Like other basanite–phonolite series, T–PV rocks are REE rich. Mafic rocks (Fig. 11a) are light REE (LREE) enriched (La_N/Yb_N ~21), with small positive Eu anomalies (Eu/Eu*). PVS and PTS plagioclase basanites and phono-tephrites have slightly lower positive Eu/Eu* and are medium REE (MREE) depleted compared with the mafic rocks. PVS tephri-phonolites show MREE depletion, with larger positive Eu anomalies (Fig. 11b). PVS phonolites (units mb[1–4]) show flattening of the heavy REEs (HREEs) and strong negative Eu anomalies. PTS tephri-phonolites show greater MREE depletion, less LREE and HREE enrichment, and similar Eu anomalies to PVS examples (Fig. 11c). PTS phonolites show less systematic REE variations than PVS examples, and smaller negative, or positive, Eu anomalies.

PETROGENESIS

The new data support fractional crystallization as an important process of differentiation for T–PV magmas (see Ridley, 1970; Araña et al., 1989). However, systematic petrological contrasts define two lineages which cannot be related by a common fractionation scheme (PTS and PVS). Contrasting lineages are common in alkaline volcanic systems and several explanations have been proposed. First, they may develop by partial melting directly, depending on source and anatectic processes (Bailey & Macdonald, 1987). Second, compositional variations among parental magmas may be amplified by fractionation to yield contrasting suites (Coombs & Wilkinson, 1969; Wilson et al., 1995), particularly if near a thermal divide (Yoder & Tilley, 1962; Kushiro, 1979). Third, bifurcation may result from a range of contamination processes, including magma mixing (McBirney, 1980), assimilation (McBirney, 1979; Foland et al., 1993), and contamination by small melt fractions, fluids or solid residues (Macdonald et al., 1987; Freundt & Schmincke, 1995). Fourth, a parental magma may fractionate under different physico-chemical conditions to yield contrasting series (e.g. Kyle, 1981; Wörner & Schmincke, 1984; Kyle et al., 1992). Here, the role of fractional crystallization is assessed qualitatively using geochemical indicators and modal data to monitor the involvement of participating mineral phases, and quantitatively using major and trace element modelling. Where fractionation is unable to account for observations, the roles of other processes are explored.

Fractionation models

Fractionation is tested using major element least-squares mass-balance (Bryan et al., 1969) and trace element fractionation models (Arth, 1976). The basanite–phonolite transition is modelled in steps, using analysed mineral compositions to identify possible bulk extracts (see Kyle, 1981; Wörner & Schmincke, 1984; Le Roex et al., 1990; Kyle et al., 1992). These extracts are used to model trace element behaviour assuming Rayleigh fractionation. Mineral–melt distribution coefficients (D) are taken from the literature and allowed to vary between models (Table 4). Criteria for the acceptability of D values are: (1) they are within the range of published values; (2) for a given mineral, they vary systematically between elements, compared with similar systems where D values are known (e.g. Le Marchand et al., 1987); (3) for each mineral, D values vary systematically from model to model. Results of selected models are given in Table 5.

Mafic rocks (>5 wt % MgO)

This section aims to constrain (1) the relationship between T–PV basanites and alkali basalts, and (2) the parental magmas of the PVS and PTS.

Teide–Pico Viejo basanites and alkali basalts

T–PV basanites and alkali basalts (unit cf[1]) have mg-numbers of 57–63 and 63–67, respectively, with the alkali basalts having higher SiO_2, MgO, Ni and Cr, and lower TiO_2, Fe_2O_3*, Na_2O, P_2O_5 and Sr than the basanites (Figs 6–8). T–PV basanites and alkali basalts have high
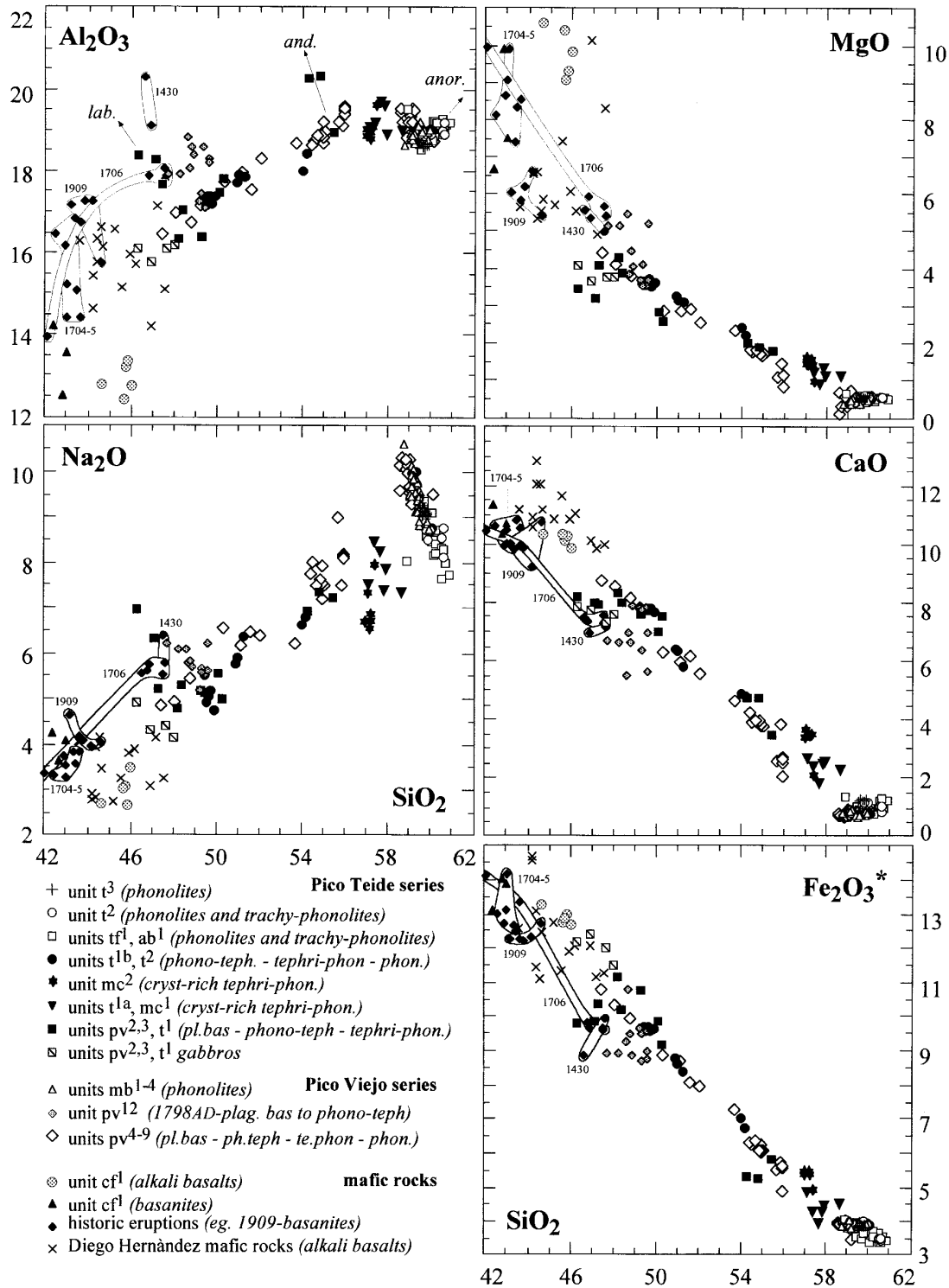
Fig. 6. Variation of selected major element oxides vs SiO₂ (wt %) for T–PV rocks, and historic and Diego Hernàndez mafic rocks [additional data after Mitjavila (1990), Cabrera (1981) and Garcia-Moral (1989)]. Fe₂O₃*, all Fe as Fe₂O₃. Seventeen analyses of unit pv⁷ phonolite (Balcells & Hernàndez-Pacheco, 1989) are included. Historic 1798 products (unit pv¹²) are plotted separately, with seven analyses from Garcia-Moral (1989). Scatter to high Al₂O₃ in PTS plagioclase basanites, tephri-phonolites and phonolites is consistent with labradorite (lab), andesine (and) and (anor) accumulation, respectively (a). Analytical errors (2σ) estimated from six duplicate analyses typically within symbol size.
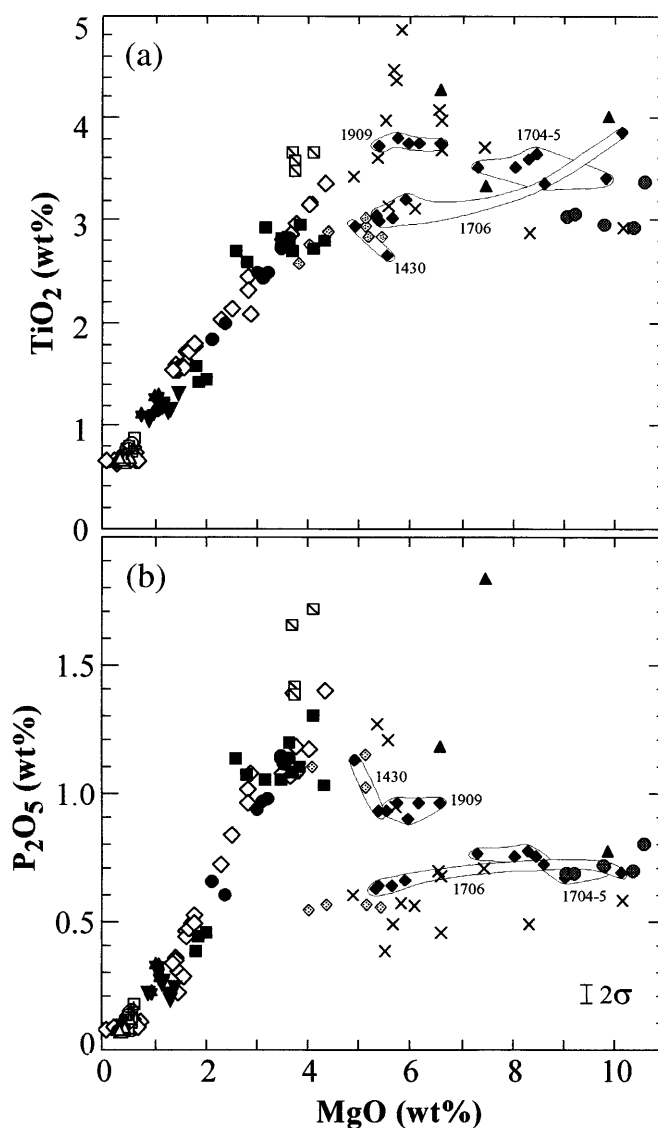
Fig. 7. (a) Variation of TiO_2 vs MgO. (b) Variation of P_2O_5 vs MgO. Symbols and errors as for Fig. 6.

CaO/Al_2O_3 ratios (0·77–0·84), compared with historic basanites (8–19% ne, *mg*-number 41–65, CaO/Al_2O_3 0·35–0·76) and magnesian Diego Hernàndez basalts (2–14% ne, *mg*-number 53–67, CaO/Al_2O_3 0·55–0·80), reflecting their uniformly lower Al_2O_3 contents (Fig. 6). The higher Al_2O_3 contents of the Diego Hernàndez and historic suites may reflect contamination by felsic magmas, as both were erupted during times of significant phonolitic magmatism.

T–PV mafic rocks do not represent primary magmas, as none are in equilibrium with mantle olivine (Roedder & Emslie, 1970) and most have accumulated phenocrysts of ol and cpx. All are somewhat evolved on the basis of *mg*-numbers. A fractionation relationship between the basanites and alkali basalts is inconsistent with their diopside-bearing phenocryst assemblages and their similar CaO/Al_2O_3 ratios. An assimilation–fractional crystallization process involving modification of basanite by low CaO/Al_2O_3 felsic partial melts to form alkali basalt (see Briot *et al.*, 1991) is similarly unlikely. There are no systematic contrasts in incompatible or REE geochemistry between the alkali basalts and basanites, and they are best interpreted as resulting from ol + cpx ± mt fractionation of primary magmas formed by different degrees of partial melting of a common mantle source (e.g. Hirose & Kushiro, 1993).
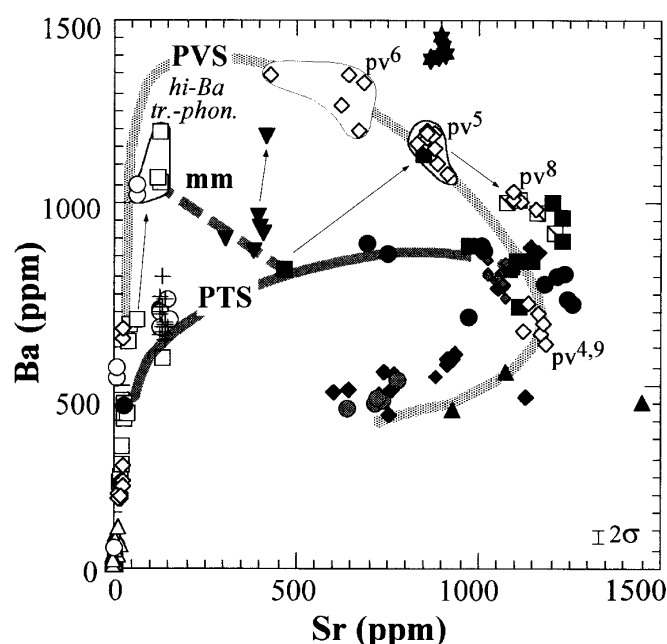
Fig. 8. Variation of Sr vs Ba. Thick continuous line (light shading), Pico Viejo series; thick continuous line (dark shading), Pico Teide series; thick dashed line (mm), magma mixing to yield crystal-rich tephri-phonolites. Thin arrows, feldspar accumulation. Symbols and errors as for Fig. 6.

Parental magmas of the Pico Teide and Pico Viejo series

The variations of Sr vs Ba, and Nb vs Zr, Rb and Y suggest that the PTS and PVS bifurcate from a common parental lineage (Figs 8 and 9). A similar relationship is seen in the behaviour of MgO vs K/Rb (Fig. 12). Plagioclase basanites of the PTS and PVS have similar K/Rb ratios (~380), whereas more evolved rocks diverge at lower MgO. The parental magma for the PTS and PVS should also have K/Rb ~380, as kaersutite, which has high K/Rb (Kesson & Price, 1972), is not a phenocryst phase in T–PV rocks more mafic than phono-tephrite (~4% MgO). T–PV basanites have appropriate K/Rb ratios (~380), whereas T–PV alkali basalts exhibit lower K/Rb (330–360), suggesting that an evolved basanite is directly parental to both the PTS and PVS. Although historic basanites generally have higher K/Rb ratios than T–PV examples, the 1909 evolved basanite is analogous to such a composition and is used in fractionation models below.

Pico Viejo series

The petrogenesis of the PVS is considered in steps, from primitive and evolved basanite (unit cf[1]/historic), through plagioclase basanite (units pv[4,9]), phono-tephrite (units pv[4,12]), mafic tephri-phonolite (unit pv[5]), and felsic tephri-phonolite (unit pv[6]), to phonolite (units pv[7], mb[1–4]).

Basanites and PVS intermediate rocks

Magnesian basanite to plagioclase basanite. Fractionation models involving basanitic parental magmas were successful in reproducing plagioclase basanites whereas those involving alkali basalts were not ($\Sigma R^2 \gg 1$). Model A (Table 5) indicates that the transition can largely be accounted for by ~41% fractionation of ol + cpx + mt + ap. The incorporation of plag (An_{66}) in model B better reproduces the observed Sr abundances. Although P_2O_5 and Sr contents are higher in the plagioclase basanites than the basanites, the removal of minor ap + plag is indicated by decreasing P_2O_5 (Fig. 7b), decreasing Sr/Ba (Fig. 8), and decreasing Eu/Eu* (Fig. 13a). Decreasing Sm/La (Fig. 13b) is ascribed to ap + cpx removal. Sm/Lu ratios are similar to parental basanites (Fig. 13c), consistent with the absence of kr. Models C and D (~53% crystallized) provide a two-step approach which, despite poor trace element fits for 1909 basanite, indicates the early importance of ol + cpx + mt fractionation and the later entrance of plag + ap.

Plagioclase basanite to phono-tephrite. This transition involves a fractionating assemblage of ol + cpx + mt + plag + ap + kr. Model E (Table 5) gives low major and trace element residuals for ~13% fractionation of the observed assemblage, although slightly overestimating the REEs. The entrance of kr causes a fall in K/Rb at ~4% MgO (Fig. 12) and may contribute to the upward inflection in Eu/Eu* at a chondrite-normalized La content (La_N) ~190 (Fig. 13a).
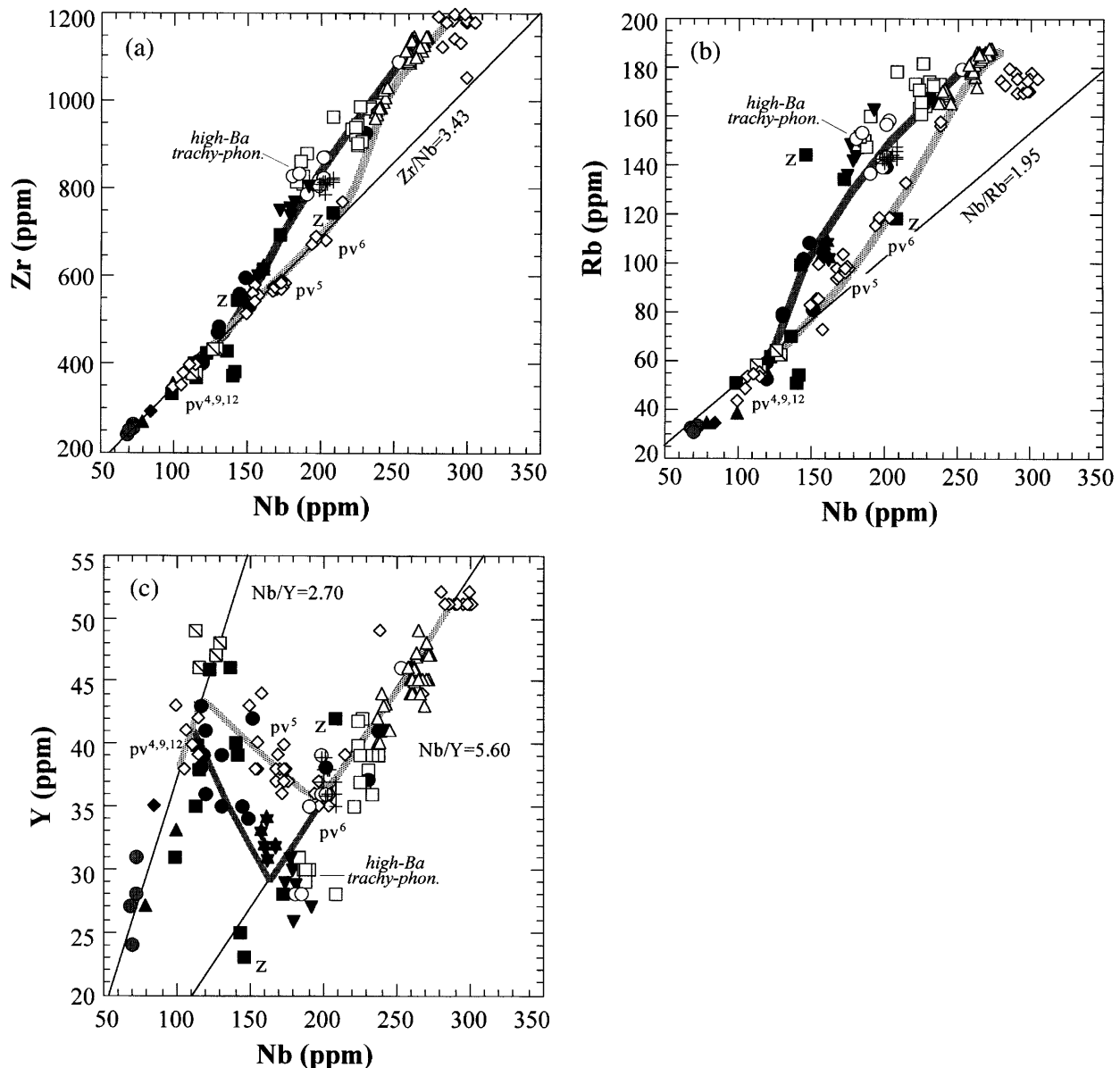
Fig. 9. Selected trace element variations. (a) Nb vs Zr; (b) Nb vs Rb; (c) Nb vs Y. Thick lines showing PVS and PTS are as for Fig. 8. Lines of constant element ratios bisect the origin. Zeolitized PTS tephri-phonolites labelled 'z'. Other symbols and errors as for Fig. 6.

Phono-tephrite to mafic tephri-phonolite. Good major and trace element fits in model F (Table 5) suggest that this transition can be accounted for by ~37% fractionation of the observed amphibole–plagioclase (An_{37}) dominated extract. MREE depletion is ascribed to removal of cpx + kr + ap. Increasing Eu/Eu* (Fig. 13a) is attributed to removal of kr + ap rather than accumulation of plag, because Sr decreases (Fig. 8) whereas Y shows a downward inflection (Fig. 9c). Enrichment in Lu (~32%) over La (~18%) is attributed to the removal of HREE-poor kr (Figs 13b and c). No model, however, could

yield the observed Rb and Ba abundances, which exceed those predicted for bulk $D^{(Rb,Ba)} = 0$, suggesting selective enrichment of mafic tephri-phonolites in Rb (Fig. 9b), and to a lesser extent Ba (Fig. 14).

Mafic tephri-phonolite to felsic tephri-phonolite. Model G yields low major and trace element residuals for ~16% fractionation of a kr-plag (An_{17}) dominated extract. Decreasing Eu/Eu* at near-constant La between units pv^5 and pv^6 (Fig. 13a) is consistent with the increased compatibility of Eu and La in sodic plag (Noble *et al.*, 1979).
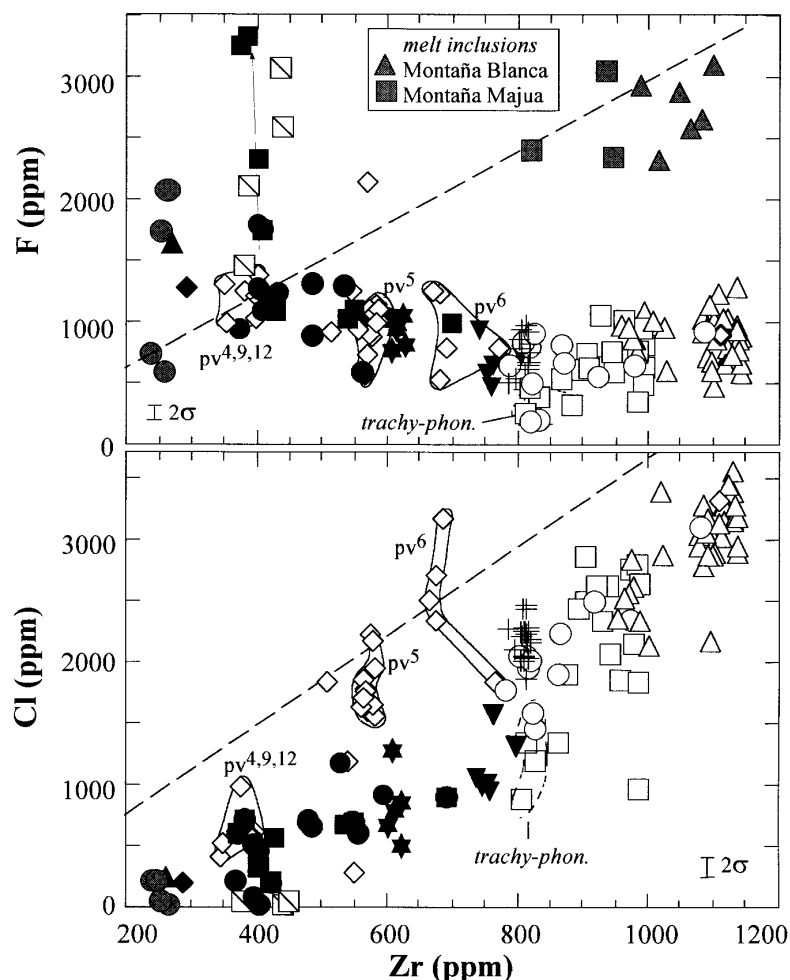
Fig. 10. Halogen abundances. The lines of F/Zr = 3 and Cl/Zr = 3·7 are shown for reference. No data for DH basalts, historic basanites (except 1909) and unit pv[7]. (a) Zr vs F; phonolite melt inclusion data included. Arrow shows apatite accumulation. (b) Zr vs Cl. Symbols and errors as in Fig. 6. (Note differences in Cl contents between PVS and PTS intermediate compositions at similar Zr.)

Phonolites

PVS phonolites (units pv[7] and mb[1–4]) are considered to derive from tephri-phonolite by fractionation of afsp + bt + cpx + mt + ap ± ilm ± titan. A maximum in Ba among felsic tephri-phonolites (unit pv[6]; Fig. 14) occurs before the onset of afsp fractionation (see Zielinski, 1975; Storey, 1981). PVS phonolites show strong depletion in Sr and Ba (Fig. 8), and negative Eu anomalies (Fig. 11) as a result of extensive feldspar removal. Flat HREEs (Fig. 11) and a decrease in K/Rb (Fig. 12) reflect the removal of kr and bt in the evolution of the phonolites. Increasing Zr/Nb within the phonolites (Fig. 9a) is consistent with the late-stage fractionation of titanite (Wolff, 1983). PVS phonolites show a strong decrease in Eu/Eu*, a weak reduction in La, and a strong reduction in Sm at near-constant Lu, followed by late-stage enrichments in La, Sm and Lu (LREEs > MREEs > HREEs) at near-constant Eu/Eu* (Fig. 15). These variations are consistent with afsp + titan + ap fractionation followed by late-stage removal of an ap-poor, titan-bearing assemblage.

Model H1 (Table 5b) tests the derivation of unit pv[7] phonolite and gives 37% fractionation of an appropriate assemblage. High major element residuals for Na, K and Al reflect the use of a single feldspar composition. For unit mb[3] phonolite, model H2 yields acceptable major element fits for 54% fractionation of an assemblage also including titanite. Titanite is involved only at a late stage, and may influence trace elements and REEs more markedly than major elements (Wolff & Storey, 1983).

Development of peralkalinity. Fractionation of cpx + plag + kr drives intermediate PVS lavas toward peralkaline compositions (Fig. 15), whereas afsp + bt
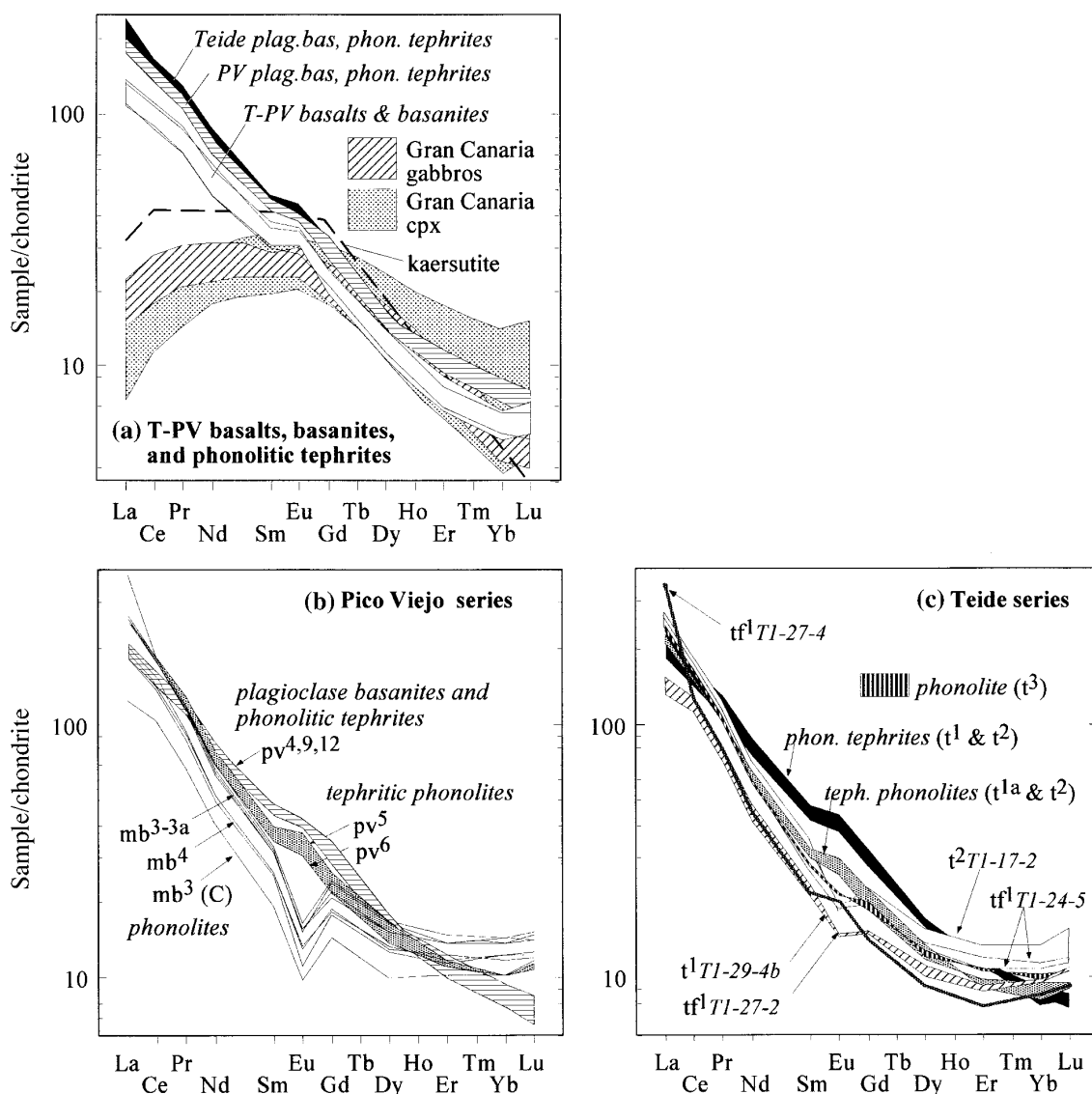
Fig. 11. Chondrite-normalized REE patterns. Individual samples shown as lines, with related samples grouped into ornamented fields. (a) Mafic and intermediate T–PV rocks (this study), gabbros and clinopyroxene separates from Gran Canaria Miocene (Freundt & Schmincke, 1995), kaersutite megacryst, Massif Central (Liotard *et al.*, 1983). (b) PVS plagioclase basanites and phono-tephrites (as a), tephri-phonolites and phonolites. (c) PTS plagioclase basanites and phono-tephrites (as a), tephri-phonolites and phonolites. Chondrite normalization constants from Masuda *et al.* (1973).

fractionation causes the phonolites to evolve toward greater peralkalinity at lower SiO_2 (Carmichael, 1964, 1967; Macdonald, 1974). This trend is only weakly counteracted by fractionation of peralkaline salite. PVS and PTS phonolites define distinct compositional groups (Fig. 15 inset). Differences in peralkalinity can be attributed to variations in mineral proportions removed over the intermediate compositional stage. The trend of PVS (MB) phonolites can be explained by a combination of kr fractionation from tephri-phonolite to phonolite,

followed by the fractionation of afsp + bt in the phonolites.

Pico Teide series

Older (units pv[2,3], t[1]) and younger PTS intermediate products (units t[1b,2]) exhibit similar chemical variations, including a lack of Ba enrichment compared with the PVS, and both are associated with comparable phonolites

Table 4: Partition coefficients (D values) used in trace element fractionation models

(a) Mafic rocks and Pico Viejo series

Model:	oliv.	pyroxene				amph.			feldspar				Fe–Ti oxides					apatite				biot.
	A–F, J	A–E	F	G	H	E–F	G	H	A–E	F	G	H	A–D	E	F	G	H	A–E	F	G	H	H
Zr	0·001	0·6	0·3	—	—	0·5	0·6	—	0·04	—	0·05	0·1	0·9	—	0·5	—	—	0·001	—	—	—	0·9
La	0·001	0·09	—	—	—	0·4	—	—	0·15	—	0·3	—	0·2	—	—	—	—	5	10	—	—	0·05
Ce	0·001	0·1	—	—	—	0·5	0·3	—	0·05	—	0·20	0·25	0·3	—	—	—	—	15	12	—	65	0·02
Rb	0·001	0·01	—	0·02	—	0·1	—	—	0·08	—	0·1	0·25	0·05	—	0·1	—	—	0·01	—	—	—	2·2
Ba	0·001	0·2	0·1	0·1	—	0·5	0·2	—	0·4	0·5	1·2	5	0·4	—	0·1	—	—	0·01	—	—	—	3·5
Sr	0·001	0·08	—	0·08	—	0·5	—	—	3·25	3·75	4	9	0·1	—	0·9	—	—	3	—	—	—	0·5
Nb	0·001	0·05	—	—	—	0·1	—	—	0·005	—	0·08	0·1	3	—	—	0·1	—	0·2	—	—	1	0·1
Y	0·01	0·2	—	—	—	0·9	3	—	0·05	—	0·1	0·25	0·01	—	—	—	—	15	—	25	—	0·3
V	0·05	0·8	—	1	1·2	0·9	2·5	—	0·001	—	—	0·2	9	15	17·5	55	30	0·001	15	25	—	2
Eu	0·001	0·1	0·2	0·7	0·8	0·5	0·8	—	0·3	0·5	2·5	3	0·2	—	0·1	—	—	25	15	—	—	0·06

(b) Pico Teide series

Model:	pyroxene				amph.			feldspar						Fe–Ti oxides				apatite						biot.
	J	K	L	M–P	L	M	N,P	J	K	L	M	N	P	J,K	L	M	N,P	J	K	L	M	N	P	M–P
Zr	*0·3*	—	*0·1*	*0·7*	*0·2*	*0·5*	—	*0·04*	—	—	*0·1*	*0·35*	—	*0·5*	*0·2*	*0·9*	—	*0·001*	—	—	—	—	—	*1·1*
La	*0·09*	—	—	—	*0·4*	*0·2*	—	*0·15*	—	*0·2*	*0·4*	*0·45*	—	*0·2*	—	—	—	*5*	—	*25*	*15*	—	*30*	*0·05*
Ce	*0·1*	—	—	—	*0·8*	*0·3*	—	*0·05*	—	—	*0·3*	*0·4*	—	*0·3*	—	—	—	*15*	—	*25*	*20*	*40*	*35*	*0·02*
Rb	*0·01*	—	—	*0·02*	*0·1*	—	—	*0·08*	—	—	*0·1*	*0·5*	*0·15*	*0·05*	—	*0·1*	—	*0·01*	—	—	—	—	—	*3·2*
Ba	*0·2*	*0·25*	—	*0·1*	*0·25*	—	—	*0·4*	*2*	*1*	*1·2*	*6·25*	*0·45*	*0·3*	—	*0·1*	—	*0·01*	—	—	—	—	—	*3·5*
Sr	*0·08*	*0·15*	—	*0·08*	*0·2*	*0·5*	*0·1*	*3·25*	*5*	*3·75*	*9*	*8·5*	*5·4*	*0·05*	—	*0·9*	*0·1*	*3*	—	—	—	—	—	*0·75*
Nb	*0·05*	—	—	—	*0·1*	*0·2*	*1*	*0·005*	—	—	*0·1*	*0·35*	*7·1*	*1·75*	—	—	*1*	*0·2*	—	—	—	—	—	*0·1*
Y	*0·2*	—	—	*0·7*	*0·9*	*3*	*0·1*	*0·05*	—	—	*0·008*	*0·1*	—	*0·01*	—	—	*0·1*	*15*	*40*	*17*	*20*	*30*	*10*	*0·3*
V	*0·8*	—	—	*2*	*0·9*	*2·5*	—	*0·001*	—	—	—	*0·2*	—	*7*	*10*	*20*	—	*0·001*	*10*	—	*25*	—	—	*2*
Eu	*0·5*	—	—	—	*0·6*	*0·8*	—	*0·5*	*0·3*	—	*2·5*	*3*	—	*0·2*	—	*0·1*	—	*25*	*10*	—	*25*	—	—	*0·06*

Letters refer to the trace element models shown in Table 5a–c. (a) Mafic rocks and Pico Viejo series; except olivine, which is not varied between models. (b) Pico Teide series. *D* values for some phases vary between models. This is justifiable, because *D* values depend on several factors, e.g. *P, T*, bulk composition and mineral composition (Irving, 1978; Reyerson & Hess, 1978; Drexler *et al.*, 1983; Wörner *et al.*, 1983; Green, 1994). Dashes indicate no change in *D* values from the preceding model. Italicized values are those which vary between the most mafic Pico Teide series models (I; Table 5c) with respect to most mafic Pico Viejo series models (E; Table 5b). Data sources: olivine—all elements (Green, 1994); pyroxene, amphibole, feldspar, magnetite and biotite—Zr, REE, Rb, Ba, Sr empirical measurements in alkaline series (LeMarchand *et al.*, 1987), except amphibole Ba, Sr (Wörner *et al.*, 1983); Zr, Y, V (Sisson, 1994). *D* values for ilmenite assumed to equal magnetite. *D*(Nb), *D*(Y) and *D*(V) assumed to equal *D*(Ta), *D*(Yb) and *D*(Sc), respectively, except for amphibole. Apatite: REE, Y (as Yb) (Wörner *et al.*, 1983); Zr, Rb, Nb, V estimated; Sr (Watson & Green, 1981).

Table 5: Results of fractional crystallization models
(a) Mafic rocks

Model:	A	B	C	D
	primitive basanite to plagioclase basanite	primitive basanite to plagioclase basanite	primitive basanite to evolved basanite	evolved basanite to plagioclase basanite
Parent	T4-21-7	T4-21-7	T4-21-7	T1909
Daughter	T2-27-10	T2-27-10	T1909	T2-27-10
ΣR^2	0.39	0.57	0.26	0.07
F (%)	40.9	49.15	22.5	29.5
olivine	29.6	22.8	45.6	5.0
pyroxene	56.1	40.2	40.9	58.9
feldspar	—	18.6	—	19.8
amphibole	—	—	—	—
magnetite	0.611.5	13.0	6.4	14.0
ilmenite	1.20.6	3.0	6.4	0.6
apatite	1.2	2.3	0.6	1.6
Zr	4	*14*	7	0
La	9	*18*	*17*	−1
Ce	−2	0	*17*	*− 18*
Rb	*19*	*34*	*28*	−1
Ba	6	3	15	−9
Sr	27	−4	5	5
Nb	7	6	*10*	−3
Y	3	5	−5	9
V	0	−8	−1	7
Eu	—	—	—	0

(b) Pico Viejo series

Model:	E	F	G	H1	H2
	plag. bas to phon. teph	phon. teph to teph. phon. (pv[5])	teph. phon. (pv[5]) to teph. phon. (pv[6])	teph. phon. (pv[6]) to phonolite (pv[7])	teph. phon. (pv[6]) to phonolite (pv[7])
Parent	T2-27-10	T1-20-24	T1-17-12	T5-16-7	T5-16-7
Daughter	T1-20-24	T1-17-12	T5-16-7	RB-1	T2-27-3
ΣR^2	0.09	0.04	0.01	0.18	0.53
F (%)	12.6	36.6	16.3	37.3	54.0
olivine	2.3	0.16	—	—	—
pyroxene	23.8	19.0	17.4	—	—
feldspar	31.9	33.4	50.6	77.6	80.9
amphibole	26.4	29.5	25.4	—	—
magnetite	14.2	13.8	4.7	4.2	4.3
ilmenite	—	—	—	—	—
apatite	2.6	4.7	2.2	1.4	0.6
biotite	—	—	—	18.4	12.6
sphene	—	—	—	—	0.5
Zr	−3	3	−1	1	5
La	−9	*− 16*	*16*	1	−9
Ce	5	5	0	9	−9
Rb	4	*−14*	−3	−9	6
Ba	3	*−12*	−10	−6	−6
Sr	−3	−3	4	−5	−2
Nb	0	−4	2	−3	−7
Y	−8	−4	5	−8	18
V	3	−1	3	2	−6
Eu	−5	−0	2	—	50

(c) Pico Teide series

Model:	I	J	K	L	M	N	P	Q
	plag. bas to plag. bas	plag. bas (pv²) to phon. teph (pv³)	phon. teph. (pv³) to teph. phon. (t¹)	phon. teph. to phon. teph. (t²)	teph. phon. to phonolite	phonolite to evolved phonolite	phon. teph. to Ba-tr. phonolite	high-Ba-tr. phonolite to phonolite
Parent	T2-27-10	T2-28-1	T1-17-4a	T1-18-3b	TPVG-1	T1-18-11	T3-17-2	T1-27-4
Daughter	T1-28-1	T1-17-4a	TPVG-1	T1-29-5	T1-18-11	T1-17-2	T1-29-6	T1-27-2
ΣR^2	0·03	0·09	0·02	0·05	0·01	0·04	0·06	0·01
F (%)	9·9	15·8	36·8	17·1	27·0	40·0	75·0	19·8
olivine	5·0	16·6	—	—	—	—	—	—
pyroxene	29·3	19·6	27·1	32·0	11·8	—	12·3	—
feldspar	51·8	46·4	49·0	46·5	52·4	90	58·4	95·7
amphibole	—	—	—	7·5	—	—	0·8	—
magnetite	7·0	3·5	20·0	14·1	7·4	4·2	8·7	2·0
ilmenite	6·1	7·2	—	—	—	—	—	—
apatite	2·7	4·5	4·7	2·4	2·7	0·8	3·2	0·7
biotite	—	—	—	—	25·8	5·4	16·4	1·6
sphene	—	—	—	—	—	—	—	—
Zr	3	1	*-11*	2	0	0	5	1
La	-2	-5	8	25	-9	1	26	-7
Ce	-9	21	6	5	*-14*	2	***36***	-1
Rb	-3	5	***-27***	***-14***	-3	-3	-9	0
Ba	-15	3	3	0	4	3	***-45***	0
Sr	-5	0	-2	-1	4	4	*33*	0
Nb	0	7	-5	4	3	8	*86*	-5
Y	5	*-14*	7	7	2	9	***68***	*-11*
V	8	29	4	-5	*151*	1	*-25*	1
Eu	0	—	—	—	—	—	—	—

The upper part of each column gives the modelled parent and daughters and the results of major element least-squares calculations. Most of the whole-rock compositions used are given in Table 3. ΣR^2 is the sum of squared residuals for ten major elements normalized to 100% anhydrous (including trace elements). Mineral compositions were selected from either the parent or daughter. No weighting was applied to the data. F (%) is the solid fraction crystallized over the modelled fractionation step. The mineral proportions give the composition of the modelled extract in wt % recalculated to 100%. The ability of the modelled extract to reproduce the trace element characteristics of the daughter by Rayleigh fractionation is shown in the lower part of each column. D values are listed in Table 4. Figures represent the per cent difference (misfit) between modelled and observed daughter for each element. Positive numbers indicate that the model extract overestimates the concentration observed in the daughter. Numbers in italics show poor fits (>10%). Numbers in bold italics show values that cannot be reproduced by Rayleigh or *in situ* fractionation models, even for bulk D values of zero.
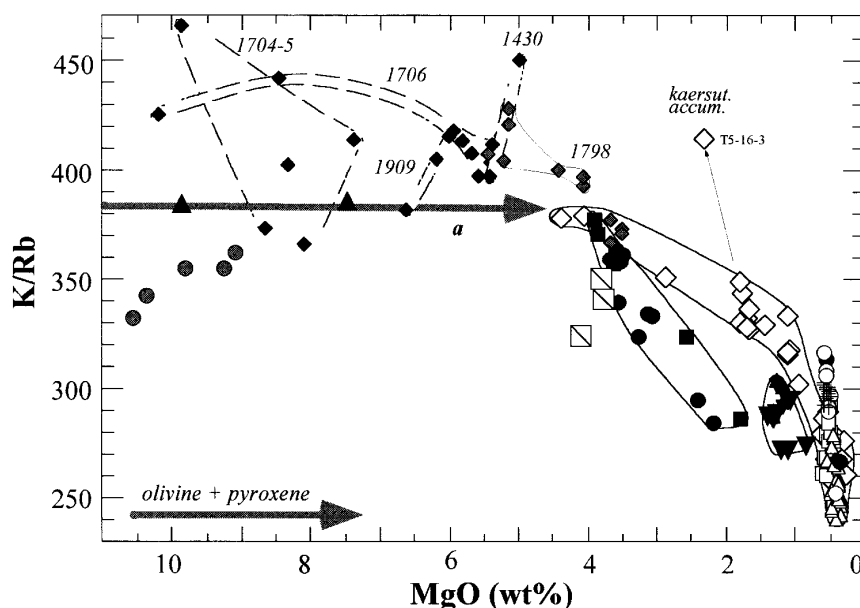
Fig. 12. Variation of K/Rb with MgO (excluding rocks showing conspicuous mineral accumulation). Thick continuous line *a* shows trend of constant K/Rb ~380 for unit cf[1] basanites parental to the PTS and PVS. (Note that the 1798 products include both evolved basanites and PVS phono-tephrite.) Pico Viejo series sample T5-16-3 has accumulated kaersutite.

and trachy-phonolites. The effects of magma mixing are identified among the younger group, and fractionation modelling (Table 5c) is applied mostly to older samples. The effects of magma mixing in the petrogenesis of the younger PTS intermediate rocks and crystal-rich tephri-phonolites (units t[1a], mc[1,2]) are discussed separately.

Older intermediate lavas and related gabbros

Older intermediate lavas (units pv[2,3], t[1]) lack kr and are dominated by skeletal high-Or plag. The plagioclase basanites have high Al_2O_3, Sr, Ba, P_2O_5 and F as a result of plag + fluor-apatite accumulation, whereas the tephri-phonolites have high Al_2O_3, CaO, and Sr and low Fe_2O_3* as a result of andesine accumulation (Figs 6–8 and 10a). Geochemical variations among non-accumulative older lavas are consistent with fractionation of the observed ol + cpx + mt + plag + ap assemblage (Figs 6 and 7). Model I (Table 5c) links PTS plagioclase basanite to the least evolved PVS plagioclase basanite (a common parent for both series), yielding low residuals for ~10% fractionation of the gabbroic assemblage. Excess Ba and Sr are attributed to plag accumulation in the daughter. Model J (Table 5c) derives phono-tephrite from plagioclase basanite to yield an acceptable fit for ~16% fractionation of the same assemblage. Poor fits for Ce, Y and V are ascribed to mt + ap accumulation. Gabbros ejected from Pico Viejo have appropriate mineralogy (plag + cpx + ol + mt + ilm + ap) and compositions to be related cumulates. They are richer in Fe_2O_3*, TiO_2,

V, P_2O_5, Y, F, and Ba than the plagioclase basanites, consistent with selective concentration of cpx + mt + ap. High Ba contents in the gabbros explain the strong Ba depletion in evolved PTS rocks (Figs 8 and 14). Model K relates early phono-tephrite to tephri-phonolite and yields good major element fits for 37% fractionation of plag + cpx + mt + ap. The inclusion of kr produced poor solutions. Extraction of a kr-free assemblage can explain the marked decreases in Sm/La and Sm/Lu shown by PTS intermediate rocks (Fig. 13b,c) but appears inconsistent with the more marked decrease in K/Rb relative to the PVS (Fig. 12). In model K, Rb and Zr concentrations in the daughter again cannot be achieved, even for bulk $D = 0$. This implies selective addition of Rb and Zr, more pronounced than proposed for Rb and Ba in the PVS (Figs 8 and 10). Contamination by incompatible element rich felsic magma or assimilation of Rb-rich zeolitized volcanics (Hart & Staudigel, 1982) are possible ways of achieving these trace element enrichments.

Young intermediate products

Young phono-tephrites and tephri-phonolites of units t[1b,2] contain minor kr and low-Or plag. They contain disequilibrium mineral assemblages, including dusty and skeletal feldspars, and mafic inclusions, consistent with a hybrid origin (Brooks & Printzlau, 1978; Gerlach & Grove, 1982; Wolff, 1985). Petrographic and mineralogical data suggest mixing between a dominant
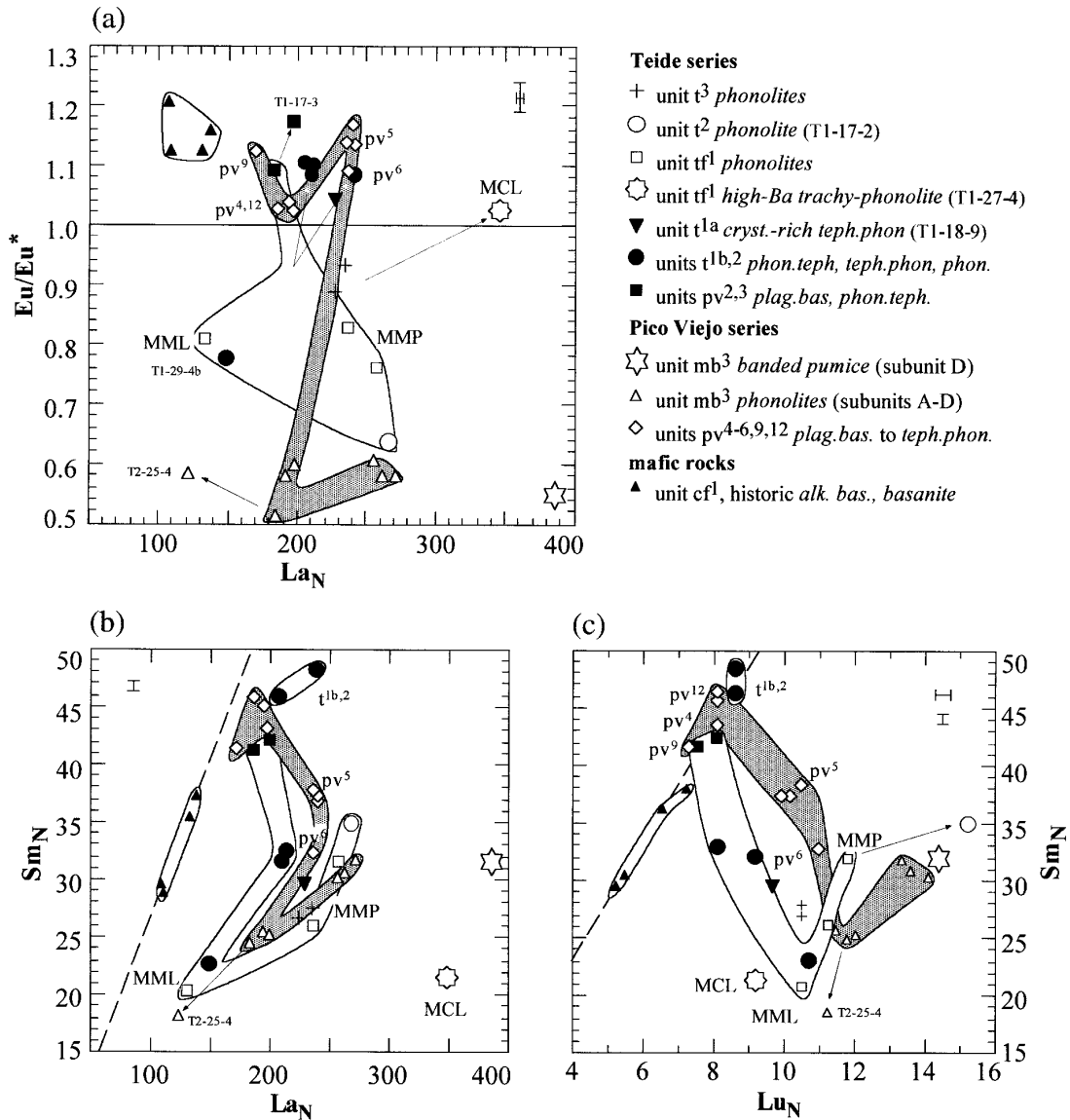
Fig. 13. Chondrite-normalized REE variations. (a) Eu anomaly (Eu/Eu* = Eu observed/Eu interpolated) vs La_N. (b) La_N vs Sm_N. (c) Lu_N vs Sm_N. La is chosen to represent the LREEs, Sm the trivalent MREEs and Lu the HREEs. Trivalent MREEs are partitioned into pyroxene, kaersutite (Fig. 11) and apatite. Kaersutitic amphibole is also HREE poor (Sisson, 1994). Eu (divalent MREE) behaves like Sr (Philpotts, 1970). Kaersutite and apatite have negative Eu anomalies, whereas feldspar has a positive Eu anomaly. Dashed lines of constant Sm/La and Sm/Lu bisect the origin. Solid arrows show inferred mineral accumulation vectors. MML, Montaña Majua lava; MMP (two samples), Montaña Majua pumice; MCL, Montaña de la Cruz trachy-phonolite; T2-25-4, unit mb³ (subunit C). Error bars show 2σ errors from three repeat analyses of tephri-phonolite.

phono-tephrite component, contributing calcic-plag + diopsidic cpx + high-Mg mt + ol + ap ± kr, and a minor tephri-phonolite component containing sodic-plag + diopsidic-salite cpx + low-Mg mt + kr + ap.

Models linking less evolved to more evolved young phono-tephrites show acceptable major element solutions for 15–17% fractionation of an assemblage including 0–18% kr (e.g. Model L, Table 5c). Rb concentrations again could not be achieved for bulk *D* values of zero. The occurrence of these products in mingled flows with phonolites supports selective enrichment in incompatible elements (Rb, Zr) as a result of contamination by felsic magma. The greater degree of incompatible element contamination exhibited by PTS magmas (Fig. 9) is
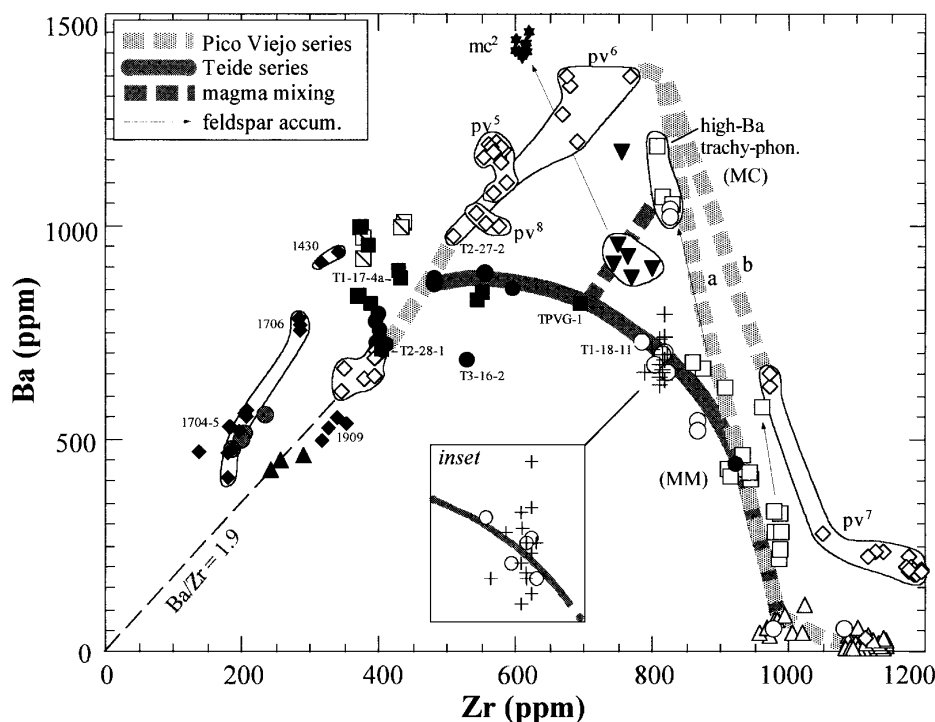
Fig. 14. Variation of Zr vs Ba for the PTS and PVS. Zr is incompatible in Tenerife magmas which lack zircon (Watson, 1979). The PTS (thick lines showing PVS and PTS as for Fig. 8) shows a trend of less pronounced Ba enrichment relative to the PVS. The PVS terminates in phonolitic trends a and b, leading to Montaña Blanca and Roques Blancos phonolites, respectively. The effects of feldspar accumulation are shown by thin arrows. The inset shows compositional contrasts between least evolved PTS phonolites of units t^2 and t^3.

consistent with a greater role for magma mixing than in the PVS.

Crystal-rich tephri-phonolites

These lavas (units tf^{1a}, $mc^{1,2}$) contain polymodal mineral populations and mafic inclusions suggesting a hybrid origin. Their mineralogy and chemistry (Figs 6–9 and 14) are consistent with mixing between older PTS tephri-phonolite (diopsidic salite + high-Or andesine + high-Mg mt + ap), and Ba-rich trachy-phonolite (afsp + salite + low-Mg mt + ap). Mixing models reproduce the crystal-rich tephri-phonolites well (Table 6), except for CaO and Sr, which is attributed to feldspar accumulation (Figs 6a and 8). Mafic inclusion morphologies and mineralogy are consistent with quenched droplets of plagioclase basanite magma (see Bacon, 1986; Blundy & Sparks, 1992).

Phonolites and trachy-phonolites

PTS felsic magmas form two main compositional groups: (1) phonolites (units tf^1, ab^1, t^2), and (2) high-Ba trachy-phonolites (units tf^1, t^2). Historic (unit t^3) phonolites are discussed separately.

Phonolites (units tf^1, ab^1, t^2). Models M and N link a putative tephri-phonolite parent to the most evolved PTS phonolite (<50 ppm Ba; Fig. 14), using the least evolved (~750 ppm Ba), non-accumulative phonolite as an intermediate (Table 5c). Major and trace element residuals are low, for a total of 67% fractionation of the observed mineral assemblage (afsp + bt + cpx + mt + ap ± ilm). Fractionation of afsp causes Ba and Sr to decrease (Figs 8 and 14), and negative Eu anomalies to develop (Fig. 11). Scatter to high Ba among PTS phonolites is attributed to minor afsp accumulation (Fig. 14). Zr/Nb ratios are similar to PTS intermediate rocks (Fig. 10a), consistent with the absence of titanite.

Trachy-phonolites (units tf^1, t^2). PTS trachy-phonolites are rich in SiO_2, Al_2O_3 and Ba, with low $Fe_2O_3^*$, TiO_2, CaO and P_2O_5 compared with PTS phonolites (Figs 6–8 and 14). They cannot be related to the phonolites by removal of afsp, as they are less peralkaline (Fig. 15). They also have higher Ba than putative intermediate parents (Fig. 14). Model P (Table 5c) shows that high-Ba trachy-phonolite cannot be derived by fractionation from such compositions as the trace elements yield a poor solution.
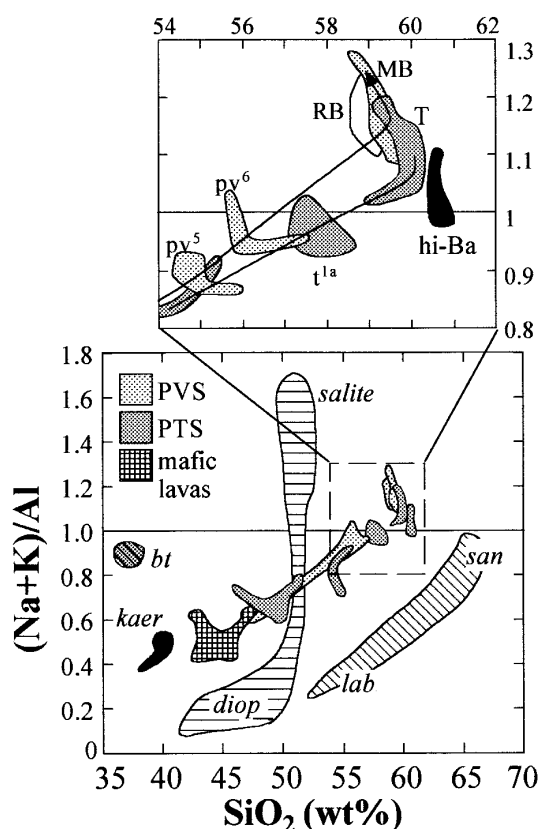
Fig. 15. Molar ([Na + K]/Al) vs SiO_2 for T–PV rocks and mineral phases: diopside (diop); salite; kaersutite (kaer); labradorite (lab); sanidine (san). Inset shows main phonolite groups: RB, Roques Blancos (PVS); MB, Montaña Blanca (PVS); T, phonolites (PTS); hi-Ba, high-Ba trachy-phonolites (PTS). Arrows show fractionation trends for PVS (upper) and PTS (lower).

The high SiO_2, Al_2O_3 and Ba and positive Eu anomalies of the trachy-phonolites (Fig. 14a) are consistent with accumulation of afsp (0·4–1·3 wt % BaO). Model Q (Table 5c) demonstrates the viability of this scheme. The model was performed in reverse to determine the extract required to derive the normal phonolite from the trachy-phonolite. Major and trace element fits are very good, suggesting that the trachy-phonolites formed by accumulation of an assemblage comprising ~95% afsp (An_{10}) and ~5% mt.

Chemical zonation of Teide phonolite reservoir. Unit tf^1 and unit t^2 felsic rocks can be related in terms of a thermally and chemically zoned chamber. The accumulative trachyphonolites are interpreted to derive from the hot, volatile-poor base of a phonolite magma layer (see Sigurdsson *et al.*, 1990), whereas contemporaneously erupted phonolites are thought to derive from the upper part of the same magma batch (see Wolff & Storey, 1983). The formation of crystal-rich tephri-phonolites, representing hybrids between accumulative trachy-phonolite and

underlying tephri-phonolite magmas (see Storey, 1981), is interpreted to have occurred in response to the trachy-phonolite magma increasing in density as a result of crystal accumulation and desiccation (Ablay, 1997).

Unit t^3 phonolites. These historic lavas resemble least evolved unit t^2 phonolites (e.g. Fig. 14) but are richer in crystals, including rounded afsp and acmitic salite (some deriving from disaggregated mineral clots), but lack biotite, similar to Tenerife syenites (Wolff, 1987; Ablay, 1997). Unit t^2 phonolite is interpreted to have been in an advanced state of crystallization when it became remobilized by mafic magma to form unit t^3. This model is consistent with high S contents (80–300 ppm) relative to other phonolites (40–120 ppm), and high Na/K (1·55–1·63; Fig. 9), consistent with late-stage Na enrichment observed in interstitial melts from syenites (Wolff, 1987). The Zr vs Ba trend (Fig. 14; inset) is interpreted to reflect partial melting of alkali feldspar. Evidence of contamination by Na, Ba and Al_2O_3 suggests that evolved

Table 6: Mixing model for generation of crystal-rich tephri-phonolite

	T1-18-9 observed	T1-18-9 calculated	Residuals
Major elements			
SiO_2	57·89	57·88	0·0072
TiO_2	1·22	1·16	0·0578
Al_2O_3	18·90	18·96	−0·0561
Fe_2O_3*	4·45	4·59	−0·4360
MnO	0·16	0·15	0·0102
MgO	1·13	1·15	−0·0240
CaO	2·56	2·36	−0·2044
Na_2O	7·88	7·76	0·1169
K_2O	4·87	4·90	0·329
P_2O_5	0·26	0·24	0·0173
ΣR^2			0·0825

	T1-18-9 observed	T1-18-9 calculated	% error
Trace element			
Zr	751	751	0
La	89	92	−4
Ce	150	148	1
Rb	143	148	−3
Ba	946	945	−1
Sr	292	400	−27
Nb	178	178	0
Y	30	31	−5
V	61	5	10

Results of major and trace element mixing model T1-18-9 = TPVG-1 (0·492) + T1-27-4 (0·508) for the generation of crystal-rich tephri-phonolite Ti-18-9 from tephri-phonolite TPVG-1 and high-Ba trachy-phonolite T1-27-4.

basanite magma erupted in 1430, 1706 and 1798 was the remobilizing agent for unit t³.

DISCUSSION

Geochemical modelling supports the derivation of both the PVS and PTS by fractional crystallization of a common evolved basanite parent magma. Geochemical contrasts can largely be accounted for by variations in the composition and proportions of the fractionating mineral assemblage, consistent with systematic modal and mineralogical differences documented between the PVS and PTS, particularly older PTS lavas. The effects of magma mixing and selective contamination have also been identified. This section considers what caused these differences in evolution, and their implications for the evolution of the T–PV magma system.

Fractionation models

Multi-step fractionation models for the PVS and PTS, in which extract variations are interpolated to approximate true modal variations with solidification index, are shown as Fig. 16. In both models the most evolved phonolites are estimated as ~13% residua of parental basanite. The first two steps are common to both series. Divergence occurs at the intermediate stage, in keeping with geochemical data. The series differ primarily in the involvement of amphibole. In the PVS, kr enters after mt, plag and ap at ~50% crystallized, and rapidly attains its maximum proportion (~30 wt %). Kaersutite continues to fractionate until the transition from plag to afsp (~70% crystallized). In the PTS, kr is absent, or low in abundance, and plag, cpx and ol dominate. Both series show similar modelled proportions of Fe–Ti oxides and ap, which are controlled essentially by individual components (Fe_3^{3+}, TiO_2, P_2O_5). Fe–Ti oxides are constant
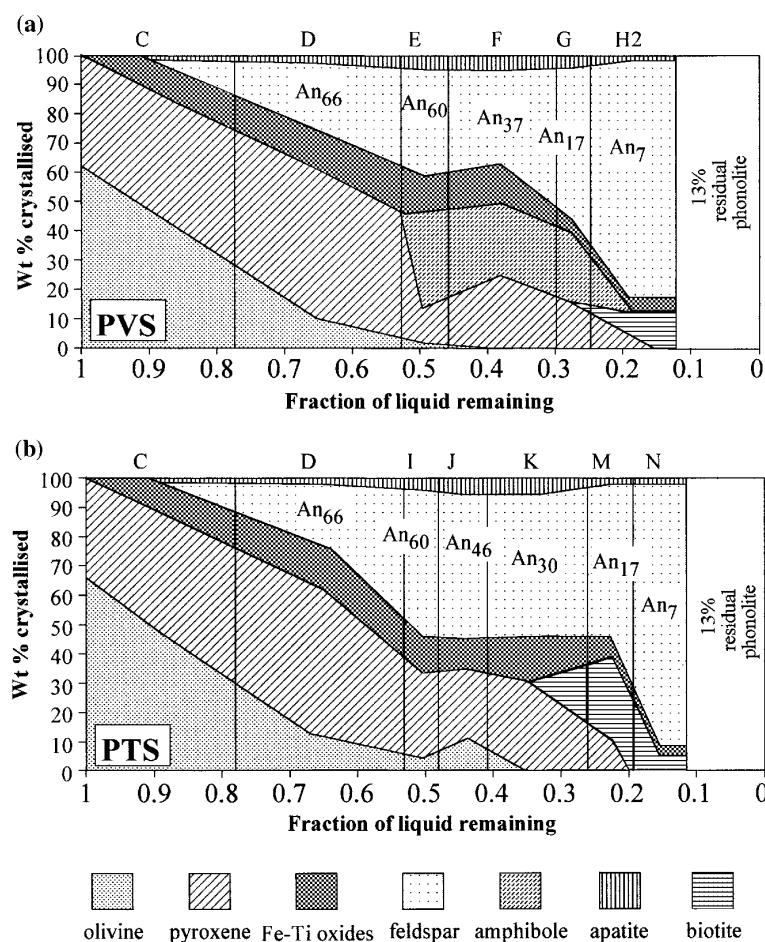
Fig. 16. Fractionation models for (a) the Pico Viejo series and (b) the Pico Teide series. The graphs are derived by interpolation of successive fractionation models listed in Table 5a–c. Each diagram shows the proportion of liquid remaining, and the proportion of each mineral in the extract. Feldspar compositions in each model also given.

at ~12 wt % until the onset of afsp and bt fractionation, when they drop to ~7 wt %. Apatite reaches a maximum of ~6% in the tephri-phonolites of both series, in keeping with chemical data. Titanite crystallizes only at a late stage in PVS phonolites.

Comparison with other suites

Kyle (1981) and Kyle *et al.* (1992) developed fractionation models for contrasting Antarctic basanite–phonolite lineages derived from a common parental basanite, the Erebus, Dry Valley Drilling Project (DVDP) and Enriched Iron series (EFS). DVDP magmas crystallize abundant kaersutite relative to the Erebus and EFS series, which are dominated by plag and cpx. Amphibole enters before plag at ~30% crystallized and reaches its highest proportion at ~65% crystallized. Wörner & Schmincke (1984) developed a seven-step model linking the Lower Laacher See phonolite to parental basanites, and suggested that the 'tephritic' lineage differed from the

'phonolitic' lineage mainly because of the greater role of kaersutite in the former. Anorthoclase phonolites of the Antarctic lineages are calculated to represent 23–25% residuals of parental basanites (Kyle, 1981), similar to the 18–19% of Tristan da Cunha phonolites (Le Roex *et al.*, 1990). These results are comparable with anorthoclase-bearing PTS phonolites (20–25% residua). The highly differentiated, sodic sanidine-bearing Montaña Blanca and Laacher See phonolites represent 13% and 9% residuals, respectively.

Significance of amphibole

Wörner & Schmincke (1984) and Kyle *et al.* (1992) described contrasting alkaline lineages which separate as a consequence of kr stability. The role of kr in alkaline series was discussed by Borley *et al.* (1971) and Kesson & Price (1972), who suggested that its removal would cause residual liquids to evolve towards peralkalinity. This is supported by the present work, which indicates

that the greater peralkalinity of PVS over PTS phonolites can be explained by the removal of kr, before afsp saturation. Kaersutite possibly suppresses cpx crystallization over this interval and causes a compositional gap from diopsidic salite to salite (see Ferguson, 1978). Absence of salite removes any tendency for the phonolite to fractionate to more aluminous compositions.

Absence of kr causes an increase in the proportions of plag, ol, cpx and bt in the PTS (Fig. 16). In the PVS, the modal proportion of ol decreases rapidly. In the PTS, the proportion of ol increases in the kr-free tephri-phonolites, explaining the occurrence of Fe-rich ol (Fo_{52}) in syeno-gabbro inclusions. These observations suggest that in the PVS, ol reacts with liquid to form kr, whereas in the PTS it remains stable to more Fe-rich compositions. Removal of Fe-rich ol contributes to the higher silica contents of PTS phonolites. Plagioclase is modally dominant in the PTS, which explains the rapid depletion of Sr and Ba relative to the PVS. The high-Or content of PTS plag justifies the slightly higher D^{Ba}(plag) values used in modelling the trace element evolution of early PTS lavas (Table 4). The increased importance of cpx (Fig. 16b) is consistent with the rapid MREE depletion shown by the PTS (Fig. 13b).

Kyle et al. (1992) suggested that decreasing K/Rb provides a good indicator of amphibole fractionation. However, K/Rb decreases more rapidly in the PTS than the PVS, despite the inferred minor role played by amphibole (Fig. 12). This difference can be explained by the selective enrichment of PTS intermediate magmas in incompatible elements, dominantly Rb (Fig. 10), while at the same time fractionating abundant Or(K)-rich plag. The higher HREE/MREE of PVS intermediate magmas (Fig. 13c) and the low, flat HREEs of PVS phonolites (Fig. 11) are better indicators of the importance of kr fractionation.

Amphibole stability

Amphibole stability depends mainly upon T, f_{O_2}, melt composition and volatile activities (Kushiro, 1970; Holloway & Burnham, 1972; Helz, 1973; Rutherford & Devine, 1988). PTS and PVS intermediate lavas have similar major element abundances, and melt composition is thus unlikely to have influenced the relative stability of amphibole. There is no evidence that f_{O_2} varied significantly between the series (Fig. 5), which cooled through the same temperature range. The activity of H_2O is therefore regarded as the major influence on amphibole stability. In ocean-island alkaline systems, as in calc-alkaline series (Gill, 1981), water is typically the dominant volatile species, as indicated by hydrous mineral phases (Kushiro, 1970; Carmichael et al., 1974), and analyses of submarine mafic–alkaline glasses (Byers et al., 1985). PVS intermediate magmas are inferred to have

fractionated amphibole under conditions of higher P_{H_2O} than PTS intermediates. This is supported by the abundance and higher Or contents of plagioclase phenocrysts in PTS intermediate lavas (Smith & Brown, 1988; Housh & Luhr, 1991; Brown, 1993). Similar high-Or and low-Or trends are noted among the feldspars of many alkaline suites (Le Roex, 1985; Price et al., 1985; Le Roex et al., 1990; Kyle et al., 1992; Freundt & Schmincke, 1995).

Volatile contents

Geochemical evidence supports the derivation of both series from a common basanite parent with the same initial water content. Given that P_{H_2O} is a function of dissolved H_2O content and P_{total}, it is salient to ask: did the PTS lose water more effectively than the PVS, or evolve at lower P_{total}, or both?

Halogen abundances and degassing behaviour

PTS and PVS rocks have low F throughout, except for those rich in accumulated fluoro-apatite, and show decreasing F/Zr with differentiation, consistent with loss of F to a vapour phase (Fig. 11a). For example, pristine melt-inclusions from phonolites have 2300–3100 ppm F, whereas matrix glasses have ~650 ppm F; indicating loss of ~80% of the initial F during eruption.

Cl abundances differ between the PTS and PVS. Cl/Zr is near constant in PVS intermediate rocks but falls in PVS phonolites, whereas in the PTS, Cl/Zr is low in the intermediate rocks and rises in the phonolites (Fig. 10b). These variations cannot simply reflect variations in Cl solubility after degassing, as the PTS and PVS have similar major element abundances. In silicic systems, Cl partitions more strongly into a hydrous vapour than F (Webster & Holloway, 1990; Webster, 1992a), whereas peralkalinity lowers D^{Cl} (Metrich & Rutherford, 1992; Webster, 1992b). Given that PTS and PVS phonolites, between which differences in peralkalinity are most marked, show similar F/Cl (Fig. 10), melt composition is unlikely to have allowed Cl to degas more effectively from the PTS than the PVS. A possible mechanism for the more efficient loss of Cl, and by implication H_2O (Anderson, 1974), from PTS intermediate magmas, is sustained open-system degassing from a shallow chamber, which would remove an increasingly high F/Cl vapour (e.g. Miller et al., 1990; Kyle et al., 1994). Late-stage sealing of the Teide chamber by syenites and syeno-gabbros can explain the increase in Cl/Zr with Zr among PTS phonolites (Fig. 10b). In contrast, PVS intermediate magmas are interpreted to have evolved under water-undersaturated conditions at greater P_{total}, and to have only exsolved a high F/Cl vapour during eruption.

Implications for the magma system

Barometric and hygrometric data indicate that the phonolites of both series evolved at low P_{total}, consistent with deriving from shallow chambers identified beneath Teide and Pico Viejo on the basis of structural data (Ablay *et al.*, 1995; Ablay, 1997). However, petrogenetic considerations suggest that the intermediate products of the two series differentiated under conditions of contrasting P_{H_2O}.

Pico Viejo sub-system

PVS phonolites yield uncalibrated pyroxene based estimates of 1–3 kbar, with more robust hygrometric results suggesting evolution at ~1 kbar P_{total} for H_2O saturation at 760°C. These estimates locate the most recent (~2 ka) shallow Pico Viejo chamber approximately at sea level (see Ablay *et al.*, 1995). PVS intermediate lavas are interpreted to have evolved at high P_{H_2O} with geobarometric evidence suggesting total pressures of 6–7 kbar. This is slightly less than the range obtained for mafic lavas (7–12 kbar) and suggests crystallization within the lower crust and uppermost mantle. Crystallization of mafic and PVS intermediate magmas at 6–12 kbar is consistent with pressure estimates of 6–10 kbar for Tenerife gabbroic and ultramafic xenoliths (Borley *et al.*, 1971; Muñoz & Sagredo, 1974). The occurrence of kr-pyroxenite xenoliths confirms that high water activities can occur under such conditions (Borley *et al.*, 1971).

Pico Teide sub-system

PTS phonolites yield uncalibrated pyroxene-based estimates of ~1–3 kbar, and more robust hygrometric estimates of 1·4–2·1 kbar P_{total} for H_2O saturation at 860°C, which locate the shallow Teide chamber at 1–3 km below sea level. Teide Flank Vent phonolites (Table 1) evolved from early intermediate magmas within the shallow chamber, in which low P_{H_2O} resulted from low P_{total} and efficient open system degassing. Pyroxene core-based pressure estimates of 6–9 kbar for these lavas appear inconsistent with evolution at low P_{total}, but can be explained in terms of polybaric evolution (Sack *et al.*, 1987). The pyroxenes are accompanied by coarse, skeletal plag phenocrysts showing a pronounced calcium spike. These features are consistent with adiabatic decompression and rapid growth at high undercooling (Smith & Brown, 1988). Older PTS intermediate lavas are interpreted to have crystallized initially at 6–9 kbar, and to have been emplaced into cool country rocks at shallow depth where they continued to differentiate at low pressure with rapid cooling and efficient crystal fractionation allowing insufficient time for pyroxene phenocrysts to re-equilibrate.

The shallow Teide chamber is interpreted to have been replenished from depth at least three times since the Teide Flank Vent phonolite eruptions, as recorded by: (1) the late admixing of plagioclase basanite inclusions within the hybrid crystal-rich tephri-phonolites (unit t^{1a}); (2) the eruption of mingled lavas containing phonolite and hybrid-intermediate components at the end of the first eruptive episode (unit t^{1b}); (3) the eruption of similar products during the second episode (unit t^2). In each case, magma containing low-Or plag phenocrysts was input into the shallow chamber, with the later inputs also containing relics of corroded kr. These replenishment events support the connection of the shallow Teide chamber to a deeper storage zone at 6–9 kbar, from which PVS intermediate magmas are derived. Periodic replenishment of the shallow Teide chamber provides an explanation for the much greater role for magma mixing during the evolution of the PTS.

The shallow Teide chamber has contained phonolitic and trachy-phonolitic magmas throughout this period, presumably as part of a long-lived zoned system. Contamination by felsic magmas provides an explanation for the enrichments in incompatible elements (Rb, Zr) seen in PTS intermediate magmas. The efficacy of the contamination process would have been increased in the case of Rb by assimilation of zeolitized volcanics affected by low-temperature alteration (Hart & Staudigel, 1982), forming the country rock around the shallow Teide chamber.

Since the second PTS eruptive episode, the felsic contents of the shallow Teide chamber congealed to a phonolitic crystal mush. The remobilization of this mush to form the historic Teide phonolite flows (unit t^3) is interpreted to have occurred in response to the recent entrance of basanite magma into the Teide chamber.

REFERENCES
Ablay, G. J. (1997). Evolution of the Teide–Pico Viejo complex and magmatic system, Tenerife, Canary Islands. Unpublished Ph.D. Thesis, University of Bristol, UK.

Ablay, G. J., Ernst, G. G. J., Martí, J. & Sparks, R. S. J. (1995). The ~2 ka subplinian eruption of Montaña Blanca, Tenerife. *Bulletin of Volcanology* **57,** 337–355.

Ancochea, E., Fuster, J., Ibarrola, E., Cendrero, A., Coello, J., Hernán, F., Cantagrel, J. & Jamond, C. (1990). Volcanic evolution of the island of Tenerife (Canary Islands) in the light of new K–Ar data. *Journal of Volcanology and Geothermal Research* **44,** 231–249.

Anderson, A. T. (1974). Chlorine, sulfur and water in magmas and oceans. *Geological Society of America Bulletin* **85,** 1485–1492.

Araña, V. & Ortiz, R. (1991). The Canary Islands: tectonics, magmatism and geodynamic framework. In: Kampunzu, A. & Lubala, P. (eds) *Magmatism in Extensional Structural Settings. The Phanerozoic African Plate.* Berlin: Springer Verlag, pp. 209–249.

Araña, V., Barberi, F. & Ferrara, G. (1989). El complejo volcanico del Teide–Pico Viejo. In: Araña, V. & Coello, J. (eds) *Los Volcanes y la Caldera del Parque Nacional del Teide (Tenerife, Islas Canarias).* Madrid: ICONA, pp. 101–126.

Arth, J. G. (1976). Behaviour of trace elements during magmatic processes—a summary of theoretical models and their applications. *Journal of Research of the US Geological Survey* **4,** 41–47.

Bacon, C. R. (1986). Magmatic inclusions in silicic and intermediate volcanic rocks. *Journal of Geophysical Research* **91,** 6091–6112.

Bacon, C. R. & Metz, J. (1984). Magmatic inclusions in rhyolites, contaminated basalts and compositional zonation beneath the Coso Volcanic Field, California. *Contributions to Mineralogy and Petrology* **85,** 346-365.

Bacon, C. R. & Hirschmann, M. M. (1988). Mg/Mn partitioning as a test for equilibrium between coexisting Fe–Ti oxides. *American Mineralogist* **73,** 57–61.

Bailey, D. K. & Macdonald, R. (1987). Dry peralkaline felsic liquids and carbon dioxide flux through the Kenya rift zone. In: Mysen, B. O. (ed.) *Magmatic Processes: Physico-chemical Principles. Geochemical Society Special Publication* **1,** 91–105.

Balcells, R. & Hernàndez-Pacheco, A. (1989). El domo-colada de Roques Blancos. In: Araña, V. & Coello, J. (eds) *Los Volcanes y la Caldera del Parque Nacional del Teide (Tenerife, Islas Canarias).* Madrid: ICONA, pp. 235–253.

Barclay, J., Carroll, M. R., Houghton, B. F. & Wilson, C. J. N. (1996). Pre-eruptive volatile content and degassing history of an evolving peralkaline volcano. *Journal of Volcanology and Geothermal Research* **74,** 75–87.

Blundy, J. D. & Sparks, R. S. J. (1992). Petrogenesis of mafic inclusions in granitoids of the Adamello Massif, Italy. *Journal of Petrology* **33,** 1039–1104.

Borley, G. D., Suddaby, P. & Scott, S. C. (1971). Some xenoliths from the alkalic rocks of Tenerife, Canary Islands. *Contributions to Mineralogy and Petrology* **31,** 102–114.

Briot, D., Cantagrel, J. M., Dupuy, C. & Harmon, R. S. (1991). Geochemical evolution in crustal magma reservoirs: trace-element and Sr–Nd–O isotopic variations in two continental intraplate series at Monts Dore, Massif Central, France. *Chemical Geology* **89,** 281–303.

Brooks, C. K. & Printzlau, I. (1978). Magma mixing in mafic alkaline volcanic rocks: the evidence from relict phenocryst phases and other inclusions. *Journal of Volcanology and Geothermal Research* **4,** 315–331.

Brown, W. L. (1993). Fractional crystallisation and zoning in igneous feldspars: ideal water buffered liquid fractionation lines and feldspar zoning paths. *Contributions to Mineralogy and Petrology* **113,** 115–125.

Bryan, W. B., Finger, L. W. & Chayes, F. (1969). Estimating proportions in petrographic mixing equations by least squares approximation. *Science* **163,** 926–927.

Byers, C. D., Garcia, M. O. & Muenow, D. W. (1985). Volatiles in pillow-rim glasses from Loihi and Kilauea volcanoes, Hawaii. *Geochimica et Cosmochimica Acta* **49,** 1887–1896.

Cabrera, M. P. (1981). Las erupciones historicas de Tenerife (Canarias). Tesis de Licenciatura, Facultad Ciences Geológicas, Universidad Complutense Madrid.

Carmichael, I. S. E. (1964). Natural liquids and the phonolitic minimum. *Journal of Geology* **4,** 55–60.

Carmichael, I. S. E. (1967). The iron–titanium oxides of salic volcanic rocks and their associated ferro-magnesian silicates. *Contributions to Mineralogy and Petrology* **14,** 36–64.

Carmichael, I. S. E., Turner, F. J. & Verhoogen, J. (1974). *Igneous Petrology.* New York: McGraw–Hill, 739 pp.

Carroll, M. R. & Blank, J. G. (1997). The solubility of H_2O in phonolitic melts. *American Mineralogist* **82,** 546–549.

Coombs, D. S. & Wilkinson, J. F. G. (1969). Lineages and fractionation trends in undersaturated volcanic rocks from the East Otago Volcanic Province (New Zealand) and related rocks. *Journal of Petrology* **10,** 440–501.

Czamanske, G. K. & Wones, D. R. (1973). Oxidation during magmatic differentiation, Finnmarka complex, Oslo area, Norway: Part 2, the mafic silicates. *Journal of Petrology* **14,** 349–380.

Drexler, J. W., Bornhorst, T. J. & Noble, D. C. (1983). Trace element sanidine/glass distribution coefficients for peralkaline silicic rocks and their implications to peralkaline petrogenesis. *Lithos* **16,** 265–271.

Eugster, H. P. & Wones, D. R. (1962). Stability relations of the ferruginous biotite, annite. *Journal of Petrology* **31,** 82–125.

Ferguson, A. K. (1978). The crystallisation of pyroxenes and amphiboles in some alkalic rocks and the presence of a pyroxene compositional gap. *Contributions to Mineralogy and Petrology* **67,** 11–15.

Foland, K. A., Landoll, J. D., Henderson, C. M. B. & Jianfeng, C. (1993). Formation of cogenetic quartz and nepheline syenites. *Geochimica et Cosmochimica Acta* **57,** 697–704.

Freundt, A. & Schmincke, H. U. (1995). Petrogenesis of rhyolite–trachyte–basalt composite ignimbrite P1, Gran Canaria, Canary Islands. *Journal of Geophysical Research* **100,** 455–474.

Garcia-Moral, R. (1989). Erupciones historicas en Tenerife. In: Araña, V. & Coello, J. (eds) *Los Volcanes y la Caldera del Parque Nacional del Teide (Tenerife, Islas Canarias).* Madrid: ICONA, pp. 347–358.

Gerlach, D. C. & Grove, T. L. (1982). Petrology of Medicine Lake Highland volcanics: characterisation of end members of magma mixing. *Contributions to Mineralogy and Petrology* **80,** 147–159.

Gill, J. B. (1981). *Orogenic Andesites and Plate Tectonics.* Berlin: Springer Verlag, 358 pp.

Green, D. H. (1994). Experimental studies of trace element partitioning applicable to igneous petrogenesis—Sedona 16 years later. *Chemical Geology* **117,** 1–36.

Grove, T. L., Kinzler, R. J. & Bartels, K. S. (1989). Effects of pressure on alumina substitution in igneous augite: an empirical geobarometer. *Eos Transactions, American Geophysical Union* **70,** 1401–1402.

Hart, S. R. & Staudigel, H. (1982). The control of alkalis and uranium in seawater by ocean crust alteration. *Earth and Planetary Science Letters* **58,** 202–212.

Helz, R. T. (1973). Phase relations of basalts in their melting range at $P_{H_2O} = 5$ Kb as a function of oxygen fugacity. Pt. 1 Mafic phases. *Journal of Petrology* **14,** 249–302.

Hewitt, D. A. & Wones, D. R. (1984). Experimental phase relations of the micas. In: Bailey, S. W. (ed.) *Micas. Mineralogical Society of America, Reviews in Mineralogy* **13,** 201–256.

Hildreth, W. (1979). The Bishop Tuff: evidence for the origin of compositional zonation in silicic magma chambers. In: Chapin, C. E. & Elston, W. E. (eds) *Ash Flow Tuffs. Geological Society of America Special Paper* **180,** 43–75.

Hirose, K. & Kushiro, I. (1993). Partial melting of dry peridotites at high pressures: determinations of compositions of melts segregated

from peridotite using aggregates of diamond. *Earth and Planetary Science Letters* **114,** 477–489.

Holloway, J. R. & Burnham, C. W. (1972). Melting relations of basalts with equilibrium water pressure less than total pressure. *Journal of Petrology* **13,** 1–29.

Holloway, J. R. (1987). *Igneous Fluids: Thermodynamic Modelling of Geological Materials: Minerals, Fluids and Melts.* New York: Springer-Verlag, pp. 273–293.

Housh, T. B. & Luhr, J. F. (1991). Plagioclase–melt equilibria in hydrous systems. *American Mineralogist* **76,** 477–492.

Huebner, J. S. & Sato, M. (1970). The oxygen and temperature relationships of manganese and nickel oxide buffers. *American Mineralogist* **55,** 934–952.

Irving, A. J. (1978). A review of experimental studies of crystal/liquid trace element partitioning. *Geochimica et Cosmochimica Acta* **42,** 743–770.

Johnson, M. C., Anderson, A. T. & Rutherford, M. J. (1994). Pre-eruptive volatile concentrations of magmas. In: Carroll, M. R. & Holloway, J. R. (eds) *Volatiles in Magmas. Mineralogical Society of America, Reviews in Mineralogy* **30,** 513 pp.

Jurewicz, A. J. G. & Watson, E. B. (1988). Cations in olivine; Part 1: Calcium partitioning and calcium–magnesium distribution between olivines and coexisting melts, with petrologic applications. *Contributions to Mineralogy and Petrology* **99,** 176–187.

Kawamoto, T. (1992). Dusty and honeycomb plagioclase: indicators of processes in the Uchino stratified magma chamber, Izu peninsula, Japan. *Journal of Volcanology and Geothermal Research* **49,** 191–208.

Kesson, S. E. & Price, R. C. (1972). The major and trace element chemistry of kaersutite and its bearing on the petrogenesis of the alkaline rocks. *Contributions to Mineralogy and Petrology* **35,** 119–124.

Kushiro, I. (1979). Fractional crystallisation of basaltic magma. In: Yoder, H. S. (ed.) *The Evolution of the Igneous Rocks: Fiftieth Anniversary Perspectives.* Princeton, NJ: Princeton University Press, 588 pp.

Kushiro, I. (1970). Formation of amphibole in peridotite compositions. *Carnegie Institute of Washington Yearbook* **68,** 245–246.

Kyle, P. R. (1981). Mineralogy and geochemistry of a basanite to phonolite sequence at Hut Point Peninsula, Antarctic, based on core from Dry Valley Drilling Project drillholes 1, 2 and 3. *Journal of Petrology* **22,** 451–500.

Kyle, P. R., Moore, J. A. & Thirlwall, M. F. (1992). Petrological evolution of anorthoclase phonolite lavas at Mount Erebus, Ross Island, Antarctica. *Journal of Petrology* **33,** 849–875.

Kyle, P. R., Sybeldon, L. M., McIntosh, W. C., Meeker, K. & Symonds, R. (1994). Sulfur dioxide emission rates from Mount Erebus, Antarctica. In: Kyle, P. R. (ed.) *Volcanological and Environmental Studies of Mount Erebus, Antarctica. American Geophysical Union Antarctic Research Series* **66,** 69–83.

Le Bas, M. J., Le Maitre, R. W., Streckeisen, A. & Zanettin, B. (1986). A chemical classification of volcanic rocks based on the total alkali–silica diagram. *Journal of Petrology* **27,** 745–750.

Le Maitre, R. W. (1989). *A Classification of Igneous Rocks and Glossary of Terms.* Oxford: Blackwell Scientific Publications, 192 pp.

Le Marchand, F., Villemant, B. & Calas, G. (1987). Trace element distribution coefficients in alkaline series. *Geochimica et Cosmochimica Acta* **51,** 1071–1081.

Le Roex, A. P. (1985). Geochemistry, mineralogy and magmatic evolution of basaltic and trachytic lavas from Gough Island, South Atlantic. *Journal of Petrology* **26,** 149–186.

Le Roex, A. P., Cliff, R. A. & Adair, B. J. I. (1990). Tristan da Cunha, South Atlantic: geochemistry and petrogenesis of a basanite–phonolite lava series. *Journal of Petrology* **31,** 779–812.

Liotard, J. M., Boivin, P., Cantagrel, J. M. & Dupuy, C. (1983). Mégacristaux d'amphibole et basaltes alkalins associés—problèmes de leurs relations pétrogénétiques et géochimiques. *Bulletin Minéralogique* **106,** 451–464.

Macdonald, R. (1974). The role of fractional crystallisation in the formation of the alkaline rocks. In: Sørensen, H. (ed.) *The Alkaline Rocks.* New York: John Wiley, pp. 442–459.

Macdonald, R., Sparks, R. S. J., Sigurdsson, H., Mattey, D. P., McGarvie, D. W. & Smith, R. L. (1987). The 1875 eruption of Askja volcano, Iceland: combined fractional crystallisation and selective contamination in the generation of rhyolitic magma. *Mineralogical Magazine* **51,** 183–202.

Martí, J., Mitjavila, J. & Araña, V. (1994). Stratigraphy, structure and geochronology of the Las Cañadas Caldera (Tenerife, Canary Islands). *Geological Magazine* **131,** 715–727.

Martí, J., Hürlimann, M., Ablay, G. J. & Gudmundsson, A. (1997). Vertical and lateral collapses on Tenerife (Canary Islands) and other volcanic ocean islands. *Geology* **25,** 879–882.

Masuda, A., Nakamura, N. & Tanaka, T. (1973). Fine structures of mutually normalised rare-earth patterns of chondrites. *Geochimica et Cosmochimica Acta* **37,** 239–248.

McBirney, A. R. (1979). Effects of assimilation. In: Yoder, H. S. (ed.) *The Evolution of the Igneous Rocks: Fiftieth Anniversary Perspectives.* Princeton, NJ: Princeton University Press, 588 pp.

McBirney, A. R. (1980). Mixing and unmixing of magmas. *Journal of Volcanology and Geothermal Research* **7,** 357–371.

Metrich, N. & Rutherford, M. J. (1992). Experimental study of chlorine behaviour in hydrous silicic melts. *Geochimica et Cosmochimica Acta* **56,** 607–616.

Miller, T. L., Zoller, W. H., Crowe, B. M. & Finnegan, D. L. (1990). Variations in trace metal and halogen ratios in magmatic gases through an eruption cycle of the Pu'u O'o vent, Kilauea, Hawaii: July–August (1985). *Journal of Geophysical Research* **95,** 12607–12615.

Mitjavila, J. (1990). *Applicació de techniques de geochimica isotopica i de geochronologia a l'estudi volcanologic de l'edifici de Diego Hernàndez, i la seva ralació amb la caldera de Las Cañadas, Tenerife, Canary Islands.* Unpublished Ph.D. thesis, University of Barcelona.

Mitjavila, J. & Villa, I. M. (1993). Temporal evolution of the Diego Hernàndez Formation (Las Cañadas, Tenerife) and confirmation of the age of the caldera using the $^{40}Ar/^{39}Ar$ method. *Revista de la Sociedad Geologica de España* **6,** 61–65.

Muñoz, M. & Sagredo, J. (1974). Clinopyroxenes as geobarometric indicators in mafic and ultramafic rocks from Canary Islands. *Contributions to Mineralogy and Petrology* **44,** 139–147.

Noble, D. C. (1965). Gold Flat member of the Thirsty Canyon Tuff—a pantellerite ash flow sheet in Southern Nevada. *US Geological Survey Professional Paper* **525,** 85–90.

Noble, D. C., Rigot, W. L. & Bowman, H. R. (1979). Rare earth element content of some highly differentiated ash flow tuffs and lavas. In: Chapin, C.E. & Elston, W. E. (eds) *Ash Flow Tuffs. Geological Society of America Special Paper* **180,** 77–85.

O'Neill, H. StC. (1987). Quartz–fayalite–iron and quartz–fayalite–magnetite equilibrium and the free energy of formation of fayalite (Fe_2SiO_4) and magnetite (Fe_3O_4). *American Mineralogist* **72,** 67–75.

Papike, J. J., Cameron, K. L. & Baldwin, K. (1974). Amphiboles and pyroxenes: characterisation of *other* than quadrilateral components and estimates of ferric iron from microprobe data. *Abstracts with Program, Geological Society of America Meeting 6,* Miami Beach, FL, pp. 1053–1054.

Parsons, I. (1981). The Klokken gabbro–syenite complex, south Greenland: quantitative interpretation of mineral chemistry. *Journal of Petrology* **22,** 223–260.

Philpotts, J. A. (1970). Redox estimation from a calculation of Eu^{2+} and Eu^{3+} concentrations in natural phases. *Earth and Planetary Science Letters* **9,** 257–268.

Price, N. J., Johnson, R. W., Gray, C. M. & Frey, F. A. (1985). Geochemistry of phonolites from the summit region of Mt. Kenya. *Contributions to Mineralogy and Petrology* **89,** 394–409.

Putirka, K., Johnson, M., Kinzler, R., Longhi, J. & Walker, D. (1996). Thermobarometry of mafic igneous rocks based on clinopyroxene–liquid equilibria, 0–30 kbar. *Contributions to Mineralogy and Petrology* **123,** 92–108.

Reyerson, F. J. & Hess, P. C. (1978). Implications of liquid–liquid distribution coefficients to mineral–liquid partitioning. *Geochimica et Cosmochimica Acta* **42,** 921–932.

Ridley, W. I. (1970). The petrology of the Las Cañadas volcanoes, Tenerife, Canary Islands. *Contributions to Mineralogy and Petrology* **26,** 124–160.

Righter, K. & Carmichael, I. S. E. (1996). Phase equilibria of phlogopite lamprophyre from western Mexico: biotite–liquid equilibria and *P–T* estimates for biotite-bearing igneous rocks. *Contributions to Mineralogy and Petrology* **123,** 1–21.

Roedder, P. L. & Emslie, R. F. (1970). Olivine–liquid equilibrium. *Contributions to Mineralogy and Petrology* **29,** 275–289.

Rutherford, M. J. (1969). An experimental determination of iron biotite–alkali feldspar equilibria. *Journal of Petrology* **10,** 381–408.

Rutherford, M. J. & Devine, J. D. (1988). The May 18, 1980 eruption of Mt. St. Helens 3. Stability and chemistry of amphibole in the magma chamber. *Journal of Geophysical Research* **93,** 11949–11959.

Rutherford, M. J., Sigurdsson, H. & Carey, S. (1985). The May 18, 1980 eruption of Mt St Helens 1. Melt compositions and experimental phase equilibria. *Journal of Geophysical Research* **90,** 2929–2947.

Sack, R. O. & Ghiorso, M. S. (1991). An internally consistent model for the thermodynamic properties of Fe–Mg-titanomagnetite–aluminate spinels. *Contributions to Mineralogy and Petrology* **106,** 474–505.

Sack, R. O., Walker, D. & Carmichael, I. S. E. (1987). Experimental petrology of alkalic lavas: constraints on cotectics of multiple saturation in natural basic liquids. *Contributions to Mineralogy and Petrology* **96,** 1–23.

Schmincke, H. U. (1982). Volcanic and chemical evolution of the Canary Islands. In: Von Rad, U., Kinz, K., Sarthein, M. & Siebold, E. (eds) *Geology of the Northwest African Continental Margin.* Berlin: Springer Verlag, pp. 273–305.

Sigurdsson, H., Carey, S., Palais, J. M., Devine, J. (1990) Pre-eruption compositional gradients and mixing of andesite and dacite and magma erupted from Nevado del Ruiz Volcano, Colombia, in 1985. *Journal of Volcanology and Geothermal Research* **41,** 127–152.

Sisson, T. W. (1994). Hornblende–melt trace-element partitioning measured by ion microprobe. *Chemical Geology* **117,** 331–344.

Smith, J. V. & Brown, W. L. (1988). *Feldspar Minerals, Vol. I; Crystal Structures, Physical, Chemical and Microtextural Properties*, 2nd edn. Berlin: Springer Verlag, 828 pp.

Soler, V., Carracedo, J. C. & Heller, F. (1984). Geomagnetic secular variation in historical lavas from the Canary Islands. *Geophysical Journal of the Royal Astronomical Society* **78,** 313–318.

Storey, M. (1981). Trachytic pyroclasts from Agua de Pau volcano, São Miguel, Azores: evolution of a magma body over 4,000 years. *Contributions to Mineralogy and Petrology* **78,** 423–432.

Waldbaum, D. R. & Thompson, J. B. (1969). Mixing properties of sanidine crystalline solutions: IV. Phase diagrams from equations of state. *American Mineralogist* **54,** 1274–1298.

Watson, E. B. (1979). Zircon saturation in felsic liquids: experimental results and applications to trace element geochemistry. *Contributions to Mineralogy and Petrology* **70,** 407–419.

Watson, E. B. & Green, T. H. (1981). Apatite/liquid partition coefficients for the rare earth elements and strontium. *Earth and Planetary Science Letters* **56,** 405–421.

Webster, J. D. (1992*a*). Fluid melt interactions in Cl-bearing silicate melts. *Geochimica et Cosmochimica Acta* **56,** 659–673.

Webster, J. D. (1992*b*). Water solubility and Cl partitioning in Cl-rich granitic systems: effects of melt composition at 2 Kb and 800°C. *Geochimica et Cosmochimica Acta* **56,** 679–687.

Webster, J. D. & Holloway, J. R. (1990). Partitioning of F and Cl between magmatic hydrothermal fluids and highly evolved granitic magmas. *Geological Society of America Special Paper* **246,** 21–34.

Webster, J. D., Taylor, R. P. & Bean, C. (1993). Pre-eruptive melt composition and constraints on degassing of a water-rich pantelleritic magma, Fantale Volcano, Ethiopia. *Contributions to Mineralogy and Petrology* **114,** 53–62.

Wilson, M., Downes, H. & Cebriá, J.-M. (1995). Contrasting fractionation trends in co-existing continental alkaline magma series; Cantal, Massif Central, France. *Journal of Petrology* **36,** 1729–1753.

Wolff, J. A. (1983). *Petrology of Quaternary pyroclastic deposits from Tenerife, Canary Islands.* Unpublished Ph.D. Thesis, Imperial College, University of London.

Wolff, J. A. (1985). Zonation, mixing and eruption of silica under-saturated alkaline magma: a case study from Tenerife, Canary Islands. *Geological Magazine* **122,** 623–640.

Wolff, J. A. (1987). Crystallisation of nepheline syenite in a subvolcanic magma chamber system: Tenerife, Canary Islands. *Lithos* **20,** 207–223.

Wolff, J. A. & Storey, M. (1983). The volatile content of some pumice-forming alkaline magmas from the Azores and Canary Islands. *Contributions to Mineralogy and Petrology* **82,** 66–74.

Wones, D. R. & Eugster, H. P. (1965). Stability of biotite: experiment, theory and application. *American Mineralogist* **50,** 1228–1272.

Wones, D. R. (1972). Stability of biotite: a reply. *American Mineralogist* **57,** 816–817.

Wörner, G. & Schmincke, H. U. (1984). Petrogenesis of the zoned Laacher See tephra. *Journal of Petrology* **25,** 836–851.

Wörner, G., Beusen, J. M., Duchateau, N., Gijbels, R. & Schmincke, H. U. (1983). Trace element and mineral/melt distribution coefficients in phonolites from the Laacher See Volcano (Germany). *Contributions to Mineralogy and Petrology* **84,** 152–173.

Yoder, H. S. & Tilley, C. E. (1962). Origin of basaltic magmas: an experimental study of natural and synthetic rock systems. *Journal of Petrology* **3,** 342–532.

Zielinski, R. A. (1975). Trace element evaluation of a suite of rocks from Réunion Island, Indian Ocean. *Geochimica et Cosmochimica Acta* **39,** 713–734.